Published in final edited form as:
Biochemistry. 2013 February 12; 52(6): 1062–1073. doi:10.1021/bi301675e.

The Kinetic Mechanism of Phenylalanine Hydroxylase: Intrinsic Binding and Rate Constants from Single Turnover Experiments†

Kenneth M. Roberts[‡], **Jorge Alex Pavon**[§], and **Paul F. Fitzpatrick**[‡,*]

[‡]Department of Biochemistry, University of Texas Health Science Center, San Antonio, TX 78229

[§]Department of Biochemistry and Biophysics, Texas A&M University, College Station, TX 77843

Abstract

Phenylalanine hydroxylase (PheH) catalyzes the key step in the catabolism of dietary phenylalanine, its hydroxylation to tyrosine using tetrahydrobiopterin (BH_4) and O_2. A complete kinetic mechanism for PheH was determined by global analysis of single turnover data in the reaction of PheHΔ117, a truncated form of the enzyme lacking the N-terminal regulatory domain. Formation of the productive PheHΔ117-BH_4-phenylalanine complex begins with the rapid binding of BH_4 (K_d = 65 μM). Subsequent addition of phenylalanine to the binary complex to form the productive ternary complex (K_d = 130 μM) is approximately ten-fold slower. Both substrates can also bind to the free enzyme to form inhibitory binary complexes. O_2 rapidly binds to the productive ternary complex; this is followed by formation of an unidentified intermediate, detectable as a decrease in absorbance at 340 nm, with a rate constant of 140 s^{-1}. Formation of the 4a-hydroxypterin and Fe(IV)O intermediates is ten-fold slower and is followed by the rapid hydroxylation of the amino acid. Product release is the rate-determining step and largely determines k_{cat}. Similar reactions using 6-methyltetrahydropterin indicate a preference for the physiological pterin during hydroxylation.

Phenylalanine hydroxylase (PheH) catalyzes the hydroxylation of phenylalanine to tyrosine (Scheme 1) in catabolism of phenylalanine in the liver, with tetrahydrobiopterin (BH_4) supplying the two electrons needed for the reaction (1). The 4a-hydroxypterin product subsequently loses water nonenzymatically to form the quinonoid dihydropterin (2). A deficiency in PheH activity results in the buildup of excess phenylalanine and the neurodegenerative diseases hyperphenylalaninemia and phenylketonuria (3). Liver PheH is subject to allosteric effects by both phenylalanine and BH_4 (4). The enzyme shows an initial lag in enzyme turnover that is abolished upon preincubation of the enzyme with phenylalanine (5, 6). Activation by the amino acid substrate involves binding to the regulatory domain of the enzyme (7), opening the active site for substrate binding (8). In contrast, preincubation of the enzyme with BH_4 increases the lag, inhibiting activation of the enzyme (9). Truncated forms of the enzyme lacking the N-terminal regulatory domain are not subject to these allosteric effects, showing similar activity to the activated wild-type enzyme (10, 11).

[†]This work was supported in part by grants from the NIH, R01 GM098140 (to PFF) and F31 GM077092 (JAP), and The Welch Foundation, grant AQ1245 (to PFF).

[*]Corresponding Author: Phone (210) 567-8264; Fax (210) 567-8778; fitzpatrick@biochem.uthscsa.edu.

Supporting Information Available

Tables S1, S2 and Figures S1–10 are provided in Supporting Information. This material is available free of charge via the Internet at http://pubs.acs.org.

PheH, tyrosine hydroxylase (TyrH) and tryptophan hydroxylase (TrpH) make up the aromatic amino acid hydroxylase family of non-heme iron monooxygenases (1). These enzymes all catalyze the insertion of an oxygen atom from molecular oxygen onto the aromatic rings of their amino acid substrates. The three eukaryotic enzymes are homotetramers, with each monomer comprised of an N-terminal regulatory domain, a highly conserved catalytic domain and a C-terminal tetramerization domain (11–13). In contrast, bacterial PheH is monomeric and solely comprised of the conserved catalytic domain (14, 15). The catalytic domains contain an active site iron atom bound in a facial 2-His-1-Glu arrangement (16–18), similar to the 2-His-1-carboxylate triads seen in several other metalloprotein families (19). The iron is proposed to mediate the incorporation of one atom of molecular oxygen each into the amino acid substrate and BH_4 to give the hydroxylated products (20). The conserved active sites, the requirement of a tetrahydropterin for catalysis, and observations that each of the eukaryotic enzymes can hydroxylate at least two of the three aromatic amino acid substrates (21–24) argue for a common mechanism for all three enzymes. The proposed chemical mechanism (Scheme 2) can be divided into two parts: 1) oxidation of the pterin cofactor to form the reactive hydroxylating intermediate, followed by 2) insertion of oxygen into the amino acid substrate (20). Supporting this view is the observation that pterin oxidation can become uncoupled from amino acid oxidation, either when nonphysiological amino acids are used as substrates (11, 25) or in a variety of TyrH active-site mutants (26–29). The uncoupled reaction of PheH with tyrosine produces hydrogen peroxide (30), implicating a peroxypterin intermediate such as the Fe(II)-peroxypterin intermediate in Scheme 2. Rapid-quench Mössbauer spectrometry of both TyrH and a bacterial PheH has provided direct evidence for an Fe(IV) intermediate, consistent with an Fe(IV)O species as the hydroxylating intermediate (31, 32). Hydroxylation of the aromatic amino acid is proposed to be through electrophilic aromatic substitution, based on the 1,2 shifts of substituents at the position of hydroxylation (25, 33, 34), the large negative ρ-values in Hammett plots for the reactions of *para*-substituted phenylalanines as substrates for TyrH (25), and the similar inverse deuterium isotope effects for the formation of the C-O bond by all three enzymes (35–37).

A molecular understanding of the regulatory properties of phenylalanine hydroxylase will require knowledge of the intrinsic rate constants for substrate binding and catalysis and how these are modulated by allosteric effects. Similarly, an understanding of the energetics of individual steps in the hydroxylation reaction will require knowledge of the intrinsic rate constants for chemical steps. We describe here the application of single turnover methods to measure individual rate constants and determine the kinetic mechanism for rat liver phenylalanine hydroxylase. To avoid complications arising from allosteric effects, a truncated form of the enzyme lacking the regulatory domain, PheHΔ117, was employed.

MATERIALS AND METHODS

Materials

BH_4 and 6-methyltetrahydropterin ($6MPH_4$) were purchased from Schircks Laboratories (Jona, Switzerland). Leupeptin was from Peptide Institute Inc. (Osaka, Japan). Ampicillin and isopropyl β-D-1-thiogalactopyranoside (IPTG) were from Research Products International Corp. (Mount Prospect, IL). Lysozyme was from MP Biomedicals, LLC (Santa Ana, CA). Streptomycin was from Affymetrix, Inc. (Santa Clara, CA). Dithiothreitol was from Inalco, S.p.A. (Milano, Italy). Magnesium sulfate and hydrochloric acid were from EMD Millipore Corp. (Billerica, MA). Glucose was from Mallinckrodt Baker, Inc. (Phillipsburg, NJ). All other reagents were purchased from Sigma-Aldrich Co. LLC (St Louis, MO) or ThermoFisher Scientific, Inc. (Waltham, MA).

Expression and Purification of rat PheHΔ117

Rat PheHΔ117 was expressed from *Escherichia coli* in a procedure modified from previously published methods (10, 11). *E. coli* BL21(DE3) cells containing the pERPHΔ117 plasmid (11) were grown at 37 °C on LB-agar containing 100 μg/mL ampicillin. A single colony was used to inoculate 100 mL of LB containing 100 μg/mL ampicillin (LB-amp), and the culture was incubated overnight. Each of six 2.8 L Fernbach flasks containing 2.0 L LB-amp supplemented with 4.0 mM magnesium sulfate and 1.0 mM ferric chloride was inoculated with 10 mL of the overnight culture. The cultures were grown in a shaker at 37 °C and 250 rpm. At an OD_{600} of 0.3–0.5, the temperature setting was lowered to 20 °C. When the cultures reached an OD_{600} of 0.7–0.9, expression was induced with 0.5 mM IPTG (final concentration). After 20 h at 20 °C, cells were harvested by centrifugation at 6200 *g* for 15 min and protein purification was performed without delay.

Except for the chromatography, which was performed at ambient temperature, all purification steps were performed at 4 °C. The cell pellet was resuspended and lysed in 8 mL per gram of cell pellet of 100 mM HEPES, 200 mM NaCl, 100 μM EDTA, 1.0 μM leupeptin, 1.0 μM pepstatin A, 100 μg/mL phenylmethylsulfonyl fluoride (PMSF) and 300 μg/mL lysozyme at pH 7.0. The lysate was passed through an 18 gauge needle three times and then stirred for one hour. The lysed suspension was divided into 45 mL aliquots and sonicated in 6 cycles of 45 s with a Branson Ultrasonics (Danbury, CT) Sonifier 450 at 50% power and 45% duty cycle. Aliquots were kept on ice for 2 min between rounds. The sonicated aliquots were recombined and centrifuged at 38,400 *g* for 1 h. Streptomycin was added to the resulting supernatant to a final concentration of 1.0%. The solution was stirred for 30 min and then centrifuged at 38,400 *g* for 1 h. To the resulting supernatant, ammonium sulfate was added to 45% saturation, and the solution was stirred for 30 min. After stirring, the protein was precipitated by centrifugation at 38,400 *g* for 1 h. The protein pellet was resuspended in 75 mL Column Buffer A (100 mM HEPES, 100 μM EDTA, 10% glycerol, 1.0 μM leupeptin, 1.0 μM pepstatin A, 100 μg/mL PMSF, pH 7.0) and dialyzed twice against 1.0 L Column Buffer A for 12 h total. After dialysis, the protein was centrifuged at 48,400 *g* for 1 h. The supernatant was loaded onto a Q-Sepharose Fast Flow (GE Healthcare Biosciences) column (16 mm × 60 cm) equilibrated with Column Buffer A. After loading, the column was washed with 150–200 mL Column Buffer A until the absorbance at 280 nm dropped below 0.2. The protein was then eluted with a gradient of 0 to 250 mM NaCl in Column Buffer A. Eluent fractions showing greater than 95% pure PheHΔ117 by polyacrylamide gel electrophoresis in the presence of sodium dodecyl sulfate were combined, and ammonium sulfate was added to 50% saturation. The solution was stirred for 30 min and then centrifuged at 35,000 *g* for 20 min. The protein pellet was resuspended in 25–30 mL Dialysis Buffer (250 mM HEPES, 200 mM NaCl, 20 mM EDTA, 20 mM nitrilotriacetic acid, 10% glycerol, pH 7.0) and then centrifuged. The supernatant (~35 mL) was dialyzed twice against 1 L Dialysis Buffer for 24 h each to prepare apo-enzyme. The metal chelators were removed by dialyzing four times against 1.0 L Reaction Buffer (250 mM HEPES, 200 mM NaCl, 10% glycerol, pH 7.0) for a total of 24 h. The dialyzed apo-PheHΔ117 was centrifuged at 31,000 *g* for 20 min to remove any denatured protein that formed during dialysis. The concentration of active enzyme was obtained by normalizing to a specific activity of 1.2 μmol tyrosine μmol^{-1} min^{-1} at 5 °C. The iron content of the purified apoprotein was determined in a procedure modified from Gottschall *et al.* (38). PheHΔ117 (30–40 μM) was incubated with 10 mM *o*-phenanthroline plus 10 mM dithiothreitol at room temperature, and the absorbance at 510 nm was monitored until no further changes were seen (~1 h). Typically, 0.8–1.2 g of purified protein with an iron stoichiometry of 10–15% was obtained from 12 L.

Stopped-Flow Absorbance Spectroscopy

Binding and single-turnover kinetics of PheHΔ117 were monitored by UV absorbance using an Applied Photophysics (Leatherhead, UK) SX18MV stopped-flow spectrophotometer. Data collection at 248 and 318 nm was performed with a 2 mm path length; at 340 nm, the path length was 10 mm. The stopped-flow instrument was made anaerobic by incubating the flow lines with anaerobic buffer containing 35 nM glucose oxidase and 5 mM glucose at 5 °C for at least 3 h prior to each experiment. During incubation and throughout data collection, N_2 was bubbled into the water bath to prevent reabsorption of O_2 into the instrument. Tetrahydropterin stock solutions were prepared daily by dissolving the dihydrochloride salt in deionized water; the concentration was determined from the absorbance at 265 nm in 2 M perchloric acid (ε = 18,000 and 17,800 M^{-1} cm^{-1} for BH_4 and $6MPH_4$, respectively). Enzyme-substrate solutions were prepared in general as follows with substrates omitted as appropriate. Typically, 300 μM apo-PheHΔ117 and 6.0 mM phenylalanine in Reaction Buffer were placed in a tonometer with a sidearm port. A stoichiometric amount of ferrous ammonium sulfate in 2 mM HCl and a volume of tetrahydropterin stock to give a final concentration of 2.0 mM were added to a sidearm. The sidearm was then attached to the tonometer and the sealed tonometer was made anaerobic through 15 vacuum-argon cycles, with the tonometer alternating between gentle shaking and resting on ice during cycles. The contents of the tonometer and sidearm were mixed together by 8–10 gentle inversions of the contents into and out of the sidearm, and the tonometer was promptly mounted onto the stopped-flow instrument. The instrument was flushed twice with 0.4–0.5 mL of the enzyme mix to remove the glucose oxidase/glucose solution prior to loading the drive syringe for data collection. In assays that required mixing enzyme with tetrahydropterin, separate tonometers were prepared containing enzyme and pterin. Anaerobic solutions of phenylalanine in buffer were prepared by bubbling argon for at least 10 min directly into a Hamilton (Reno, NV) 12 mL Gastight syringe containing 8–10 mL of an appropriate phenylalanine solution and mounting the syringe onto the instrument immediately. Approximately 3.5 mL of solution were flushed through the instrument prior to loading for data collection. Solutions of different O_2 concentrations were prepared by mixing N_2 and O_2 with a MaxTec (Salt Lake City, UT) MaxBlend low flow medical oxygen mixer and bubbling directly into the syringe containing buffer or the phenylalanine solution. All experiments were performed at 5 °C; solutions were incubated for at least 10 min after loading onto the stopped-flow instrument before initiating data collection. The stopped-flow traces shown in figures are the averages of at least five independent traces.

Rapid-Mixing Chemical-Quench

Pre-steady state tyrosine formation was quantified in chemical quench assays using a BioLogic (Claix, FR) QFM-400 quench-flow instrument. Similar to the procedure for the stopped-flow instrument, the QFM-400 was incubated at 5 °C with anaerobic buffer containing 35 nM glucose oxidase and 5 mM glucose for a minimum of 3 h to remove oxygen. The water bath was bubbled with N_2 during incubation and data collection. Solutions of 40 μM apo-PheHΔ117, 80 μM Fe(II) and 2.0 mM tetrahydropterin were prepared as described for stopped-flow assays, except the instrument was flushed twice with 1 mL of the enzyme mix prior to loading the drive syringe. Phenylalanine-O_2 solutions were prepared by bubbling 100% O_2 into a 4.0 mM phenylalanine solution in a 12 mL Gastight syringe on ice for at least 10 min to give a concentration of 1.9 mM O_2. The syringe was immediately mounted onto the instrument after bubbling. Approximately 4 mL of the phenylalanine-O_2 solution was flushed through the instrument prior to loading for data collection. A quench solution of 2 M HCl was loaded into a third drive syringe. Assays were performed by mixing the contents of the tonometer with the phenylalanine-O_2 solution into a 3.5 μL delay line followed by quenching with acid. Reaction times were varied by changing the flow rate. The quenched reaction was collected in 0.5 mL microfuge tubes,

vortexed and centrifuged to pellet precipitated enzyme. The supernatant (100 μL) was transferred to a glass HPLC vial containing 900 μL 0.1% acetic acid and vortexed. Tyrosine was isolated on a Phenomenex Gemini-NX column (5 μm; 4.6 × 250 mm) with an isocratic mobile phase of 0.1% acetic acid at a flow rate of 1.0 mL/min. Tyrosine formation was quantified by fluorescence detection with excitation at 275 nm and emission at 303 nm.

Data Analysis

Preliminary analysis of stopped-flow data was performed using KaleidaGraph (Synergy Software, Reading, PA) for fits to individual traces and Igor Pro (Wavemetrics, Lake Oswego, OR) for global fitting of multiple traces. Rapid-quench data were fit using KaleidaGraph. KinTek Explorer (39) (KinTek Corporation, Austin, TX) was used to perform global analyses of multiple experiments using singular value decomposition to define kinetic models and elucidate intrinsic rate values. The FitSpace Explorer (40) package of KinTek Explorer was used to evaluate the statistical validity of individual models. FitSpace Explorer estimates the confidence in best-fit values by determining the sum square error for all pairs of parameters, allowing all other parameters to float. The reported confidence intervals are the ranges of values for each parameter in which best fit curves give X^2 values below a specified X^2 threshold. The X^2 thresholds are multiples of the global best fit X^2 value, e.g., the confidence intervals for a X^2 threshold of 1.2 are the range of values for which the fits have X^2 values no more than 20% greater than the lowest X^2 value. For each model, KinTek Explorer generates an estimated X^2 threshold to be used in FitSpace analyses. The X^2 thresholds reported in this study are at least two-fold larger than the threshold values estimated by KinTek Explorer. For all analyses with KinTek Explorer, the extinction coefficient for free BH_4 was fixed at 1400 and 750 M^{-1} cm^{-1} at 335 and 340 nm, respectively.

RESULTS

Spectral changes upon binding of substrates to PheHΔ117

The kinetics of binding of phenylalanine and BH_4 to PheHΔ117 were analyzed using stopped-flow absorbance spectroscopy. Initially, PheHΔ117 plus BH_4 were mixed with phenylalanine in the absence of oxygen at 5 °C. The resulting stopped-flow traces showed an increase in absorbance between 315 and 360 nm within the first 100 ms (Figure 1A). This absorbance change is consistent with formation of a PheHΔ117-BH_4-phenylalanine ternary complex. The maximal absorbance change was observed at 330 nm (Figure 1B); however, due to the high absorbance from the pterin at this wavelength, binding reactions were routinely monitored at 340 nm, unless otherwise noted.

To confirm that the observed absorbance change was due to ternary complex formation, experiments were performed using different combinations of PheHΔ117, BH_4 and phenylalanine. Figure 2 shows the absorbance traces at 340 nm when one or both substrates is mixed with the enzyme. The addition of phenylalanine to free enzyme does not result in a change in absorbance at 340 nm. In contrast, mixing free enzyme with BH_4 results in a small absorbance increase within the first 5–10 ms. Mixing free enzyme with BH_4 plus phenylalanine results in a much larger absorbance increase over the first 100 ms. A similar absorbance trace is observed upon mixing a solution of enzyme plus BH_4 with phenylalanine, indicating that both orders of addition result in formation of the same species. Interestingly, addition of BH_4 to a solution of enzyme plus phenylalanine results in a slower change in absorbance. In all experiments containing both substrates, the total absorbance change was independent of the order of mixing. Similar assays with $6MPH_4$ in the presence of phenylalanine gave traces showing only half the absorbance change that was seen with

BH_4 and no absorbance change with either $6MPH_4$ or phenylalanine alone, precluding investigation of the binding kinetics of the PheHΔ117-$6MPH_4$ system.

Kinetics of Binding of BH_4 to PheHΔ117

To evaluate the kinetics of BH_4 binding to PheHΔ117, stopped-flow experiments were performed in which PheHΔ117 was mixed anaerobically with increasing concentrations of BH_4 (|E vs BH_4|). The reaction was monitored at 335 nm. In all cases, the increase in absorbance was biphasic (Figure 3A). A two-phase model was fit to the stopped-flow traces using eq 1 (Figure S1A). The resulting values for the rate constant for the first phase (k_{1obs}) showed a linear dependence on the concentration of BH_4 (Figure 3B); these were fit with eq 2 to give apparent on and off rates of 390 ± 40 mM^{-1} s^{-1} and 130 ± 30 s^{-1}, respectively. The value of the rate constant for the second phase (k_{2obs}) showed no apparent concentration dependence and had an average value of 50 ± 14 s^{-1} (Figure 3B). The observation of two distinct phases indicates the existence of two unique E-BH_4 complexes in the PheHΔ117-BH_4 binding reaction. Scheme 3 shows two possible kinetic mechanisms involving two E-BH_4 complexes. In the first, BH_4 binds to the enzyme forming an initial binary complex, E'-BH_4, which then undergoes rearrangement in a second step to form an alternate complex, E"-BH_4 (Scheme 3A). In the second mechanism, the two binary complexes arise from two independent binding steps (Scheme 3B). To determine the binding mechanism, Schemes 3A and 3B were fit to the stopped-flow data using KinTek Explorer (39) (Figure S1B)[1]. The values for the intrinsic rate constants for each model are given in Table 1. Though the rate constants are clearly distinct for the two mechanisms, fits for the two gave identical curves and X^2 values.

$$A_t = A_0 + \sum (A_i e^{-k_{iobs} t}) \quad (1)$$

$$k_{1obs} = k_{-1} + k_1([E]+[S]) \quad (2)$$

Kinetics of Ternary Complex Formation

The kinetics of formation of the PheHΔ117-BH_4-phenylalanine ternary complex were initially investigated by anaerobically mixing a solution of PheHΔ117 plus BH_4 with increasing concentrations of phenylalanine (|E-BH_4 vs Phe|). The absorbance changes at 340 nm were again biphasic (Figure 4A), so that the data were fit with eq 1 (Figure S2). The rate constant for the initial phase (k_{1obs}) showed a linear dependence on the phenylalanine concentration (Figure 4B) and was fit with eq 2 to obtain apparent on and off rate constants of 24 ± 4 mM^{-1} s^{-1} and 26 ± 6 s^{-1}, respectively. The second phase (k_{2obs}) showed a hyperbolic dependence on the concentration of phenylalanine (Figure 4C). Fitting these data with eq 3 using the values for k_1 and k_{-1} calculated from Figure 4B gave values for k_2 and k_{-2} of 5 ± 1 s^{-1} and 6.6 ± 0.7 s^{-1}, respectively.

[1]For reactions exhibiting multiple phases, the relationship between the individual rate constants and the rate constants derived from direct analysis of the phases depends on the specific kinetic mechanism. Moreover, in several of the experiments described here, the concentrations of substrate and enzyme differ by less than 5-fold, so that analyses as sequential first-order processes may not yield reliable values for the corresponding rate constants for the individual phases. Consequently, initial analyses using eq 1 were carried out solely to establish the number of observable phases in each reaction, and analyses with eqs 2 and 3 only to determine if any phases were sensitive to the substrate concentration. In the subsequent analyses of the individual kinetic models with KinTek Explorer, no constraints were placed on the values of the rate constants. In addition, multiple starting values for the individual rate constants were used in KinTek Explorer to ensure that the fitting converged on a true minimum. Comparison of the values for the rate constants determined globally and by more traditional analytical methods demonstrates the inability of more traditional methods to accurately determine intrinsic rate constants, particularly from data arising under non-first-order conditions.

$$k_{2obs}=k_{-2}+\frac{k_2([E]+[S])}{k_{-1}/k_1+[E]+[S]} \quad (3)$$

Both of the mechanisms in Scheme 3 predict that a solution of PheHΔ117 and BH_4 will contain two enzyme-BH_4 complexes in equilibrium. The observation of two phases when phenylalanine is added suggests that phenylalanine preferentially binds to one of the binary complexes to yield an enzyme-BH_4-phenylalanine ternary complex (E-BH_4-Phe) and that a second phase arises from the slow conversion of the unproductive binary complex. Three models were considered for the formation of E-BH_4-Phe (Scheme 4). In the first, formation of the E-BH_4-Phe complex occurs through addition of phenylalanine to the terminal E-BH_4 complex in a fully sequential mechanism (Scheme 4A). In the second mechanism, phenylalanine binds to the intermediate E-BH_4 complex to form the ternary complex (Scheme 4B). In this model the second E-BH_4 complex is unreactive. The third mechanism is characterized by addition of phenylalanine to a single E-BH_4 complex in the branched enzyme-BH_4 mechanism (Scheme 4C). (Note that a model involving formation of the E-BH_4-Phe complex from E"-BH_4 is formally equivalent to the mechanism of Scheme 4C.) Using KinTek Explorer, these three models were fit to the combined data from the |E vs BH_4| and |E-BH_4 vs Phe| experiments. The fits for each model are shown in Figure S3, and the intrinsic rate constants given in Table 2. The X^2 values for the kinetic mechanisms in Schemes 4A and 4B differ by only 1%. Furthermore, the rate constants and confidence intervals are identical for the two models. The fit to the branched mechanism (Scheme 4C) gives a X^2 value that is only 10% higher, too small a change to rule out this mechanism. The values for k_3 and k_{-3} are essentially identical in all three mechanisms.

These results describe the formation of a PheHΔ117-BH_4-phenylalanine ternary complex through an ordered mechanism initiated by the binding of BH_4 to the free enzyme. However, addition of BH_4 to a solution of enzyme and phenylalanine showed slower formation of the ternary complex than other orders of mixing (Figure 2), suggesting the possibility of a dead-end enzyme-phenylalanine (E-Phe) complex. Addition of phenylalanine to a solution of free enzyme does not result in a spectral change, precluding direct analysis of the kinetics of E-Phe formation. To determine the kinetics of formation of the E-Phe complex, two complementary experiments were performed. In the first, solutions of enzyme plus three concentrations of phenylalanine were reacted with varying concentrations of BH_4 (|E-Phe vs BH_4|). The resulting stopped-flow traces (Figure 5) were independently fit with two, three or four phases using eq 1, with the values for the rate constants for each individual fit given in Table S1. Each trace fit well to a three-phase model (Figure S4); however, the values for the rate constants suggested four phases were required to collectively describe all nine traces. The values for k_{1obs} at 0.3 and 0.9 mM phenylalanine for all concentrations of BH_4 agree reasonably well with the values of 270, 510 and 750 s^{-1} expected for the first phase when enzyme is mixed with 0.3, 0.9 and 1.5 mM BH_4, respectively (Figure 3B), suggesting that this phase reflects the binding of BH_4 to the free enzyme. The values for k_{1obs} at 3.0 mM phenylalanine are an order of magnitude smaller than the values at the lower concentrations of phenylalanine, indicating that the binding of BH_4 to free enzyme is inhibited. Saturation of the enzyme as an E-Phe complex that must dissociate prior to addition of BH_4 explains these results. The values for k_{2obs} showed no apparent dependence on the concentration of either substrate and had an average value of 16 ± 4 s^{-1}. This phase may reflect the second phase in the addition of phenylalanine to the enzyme-BH_4 complex, though the value is larger than those in Figure 4C. The slowest phase (k_{3obs}) shows an inverse dependence on the concentration of phenylalanine and was not seen in the preceding experiments, suggesting this phase originates from E-Phe.

In the second experiment, both substrates were added simultaneously to the free enzyme (|E v BH_4-Phe|). Specifically, solutions of BH_4 plus three concentrations of phenylalanine were mixed with PheHΔ117 under anaerobic conditions (Figure 6). The stopped-flow traces were fit to eq 1 with four phases (Figure S5) to obtain the rate constants in Table S2. The first phase (k_{1obs}) is rapid and likely reflects the initial formation of the enzyme-BH_4 complex, though the values are larger than those seen for the first phase when 0.3 mM BH_4 is added to free enzyme (Figure 3B). The values for k_{2obs} are similar to the values for the second phase in the formation of the E-BH_4 complex (Figure 3B), suggesting this phase also represents formation of the binary complex. The values for k_{3obs} and k_{4obs} are similar to the values for the second and third phases in the previous experiment (|E-Phe v BH_4|, Table S1), respectively.

Global Analysis of Binding Kinetics

The data from all four experiments, |E v BH_4|, |E-BH_4 v Phe|, |E-Phe v BH_4| and |E v BH_4-Phe|, were fit globally with KinTek Explorer to determine the kinetic mechanism for substrate binding to PheHΔ117. Three different kinetic mechanisms (Scheme 5) were constructed by adding an unproductive E-Phe complex to the mechanisms in Scheme 4. The values for the rate constants from fits with the mechanisms in Schemes 5A, 5B and 5C are given in Table 3. The fits to the data are shown in Figures S6, S7 and 3–6, respectively. The X^2 values for the fits to the three models show a clear distinction in the quality of the fits. The mechanism in Scheme 5A yielded the worst fit of the data, with a X^2 value more than twice that for Scheme 5C. In addition, the values of the individual rate constants and their confidence intervals for the two steps in the formation of the E-BH_4 complex were large, with FitSpace calculations indicating k_1, k_{-1} and k_2 may have no upper bound, confirming that this model does not adequately represent the data. The mechanism in Scheme 5B also gave a significantly worse fit than that in Scheme 5C, with a X^2 value nearly twice as large. The confidence intervals for the rate constants for Scheme 5B were significantly larger than those for Scheme 5C, indicating that the former model is not as well defined by the data. Thus, the mechanism in Scheme 5C gives the best fit to the stopped-flow data. For all three models, the values for k_3 and k_{-3} are similar.

Kinetics of Phenylalanine Hydroxylation by PheHΔ117

The kinetics of phenylalanine hydroxylation by PheHΔ117 were evaluated using stopped-flow absorbance spectroscopy. The hydroxylation reaction was performed with both BH_4 and $6MPH_4$ to determine the dependence of the kinetics on the identity of the pterin. An anaerobic solution of PheHΔ117, phenylalanine and BH_4 or $6MPH_4$ was mixed with solutions of buffer containing increasing concentrations of O_2 (Figure 7). The enzyme and substrates were preequilibrated to avoid interference from binding. The O_2 concentration was kept below the enzyme concentration to limit the reaction to a single turnover. Formation of the 4a-HO-BH_3 (or 4a-HO-$6MPH_3$) intermediate is detectable as an absorbance increase at 248 nm and a decrease at 318 nm (35). Changes in the environment around the pterin are detectable at 340 nm, as seen for the binding complexes.

The stopped-flow traces obtained with BH_4 (Figure 7A–C) could be fit with three phases using eq 1 (Figure S8). The rate constants showed no apparent dependence on the concentration of O_2, fitting all traces with values of 49.6 ± 0.6, 9.2 ± 0.4 and 3.5 ± 0.1 s^{-1}. The traces obtained with $6MPH_4$ (Figure 7D–F) also fit well with three phases (Figure S9). Again, the rate constants showed no apparent dependence on the concentration of O_2, with values of 32 ± 2, 2.7 ± 0.9 and 2.2 ± 0.9 s^{-1}.

Rapid-Mixing Chemical-Quench Analyses

The kinetics of tyrosine formation were measured directly using chemical-quench experiments. Solutions of PheHΔ117 preincubated anaerobically with pterin were mixed with solutions of phenylalanine saturated with oxygen at 5 °C (Figure 8). The chemical-quench data with either pterin show a clear burst in tyrosine formation within the first 500 ms and were fit to eq 4 (Figure S10) to give values for k_{burst} of 8.2 ± 1.8 and 3.7 ± 0.5 s^{-1} for BH_4 and $6MPH_4$, respectively. A subsequent linear phase extending beyond the first second indicates the reaction has reached steady-state with k_{cat} values of 1.41 ± 0.03 s^{-1} with BH_4 and 0.99 ± 0.02 s^{-1} with $6MPH_4$. A burst phase in product formation is most consistent with product release being rate-limiting rather than earlier chemical steps.

$$\left(\frac{\text{Tyr}}{\text{E}}\right)_t = 1 - e^{-k_{burst}t} + k_{cat}t \quad (4)$$

Global Analysis of the Hydroxylation Reaction

The time-dependent data for hydroxylation by PheHΔ117 including the stopped-flow traces and rapid-quench data were combined to define a complete kinetic mechanism. The stopped-flow data showed three observable phases in the hydroxylation reaction with no dependence on the concentration of oxygen when either pterin was used. The rapid-quench data indicated rate-determining product release. These observations suggest a model with four steps: reversible binding of oxygen followed by two intermediate steps and product release. For the reaction with BH_4, these steps were appended to Scheme 5C to generate a complete mechanism from substrate binding to product release (Scheme 6A). This mechanism was fit to the combined data from Figures 7A–C and 8 with the rate constants for the binding steps (k_1-k_{-4}) fixed at the values in Table 3.[2] Initial evaluation with FitSpace Explorer indicated that the values for k_5 and k_{-5} were not well constrained, having no upper limit; however, the ratio for these values (k_{-5}/k_5; K_{O2}) was well defined with a value of 200 μM. FitSpace calculations were consequently performed with k_5 and k_{-5} fixed at their best fit values. The resulting values for the rate constants and confidence intervals are given in Table 4. The combined time-dependent data for the reaction with $6MPH_4$ were fit with the model in Scheme 6B. Steps for substrate binding were not included in this model as the kinetics of substrate binding were inaccessible due to the lack of a significant binding signal with $6MPH_4$. The values for the rate constants and confidence intervals are reported in Table 4. As with BH_4, the values for k_5 and k_{-5} showed no upper limit. As such, these rate constants were fixed, yielding a value for K_{O2} of 20 μM.

DISCUSSION

The present study establishes a detailed kinetic mechanism for PheHΔ117 including substrate binding, the hydroxylation reaction, and product release (Scheme 6A), with intrinsic rate constants for each step (Tables 3 and 4). These results take advantage of the ability to detect multiple binding complexes in the PheHΔ117-BH_4-phenylalanine system through changes in UV absorbance in the region between 315 and 360 nm (Figure 1). This region likely corresponds to the long wavelength edge of the tetrahydropterin absorption band, as the wavelengths are too long for phenylalanine or the aromatic amino acids in the enzyme. The contribution of BH_4 to the absorbance signal is supported by the absorbance change in the absence of phenylalanine and the lack of any signal in the absence of BH_4 (Figure 2), suggesting that the formation of the PheHΔ117-BH_4 binary complex perturbs the

[2]The mechanism in Scheme 6A was also fit to the combined data for both binding and oxidation, with all rate constants allowed to vary. The resulting values for the rate constants were nearly identical to the values reported in Tables 3 and 4.

electronic environment around the pterin. Addition of phenylalanine to the binary system to generate the PheHΔ117-BH_4-phenylalanine ternary complex further alters the environment, increasing the absorbance signal.

Comparison of the available structures of the ferrous catalytic domain of human PheH shows that the formation of the ternary complex results in several structural changes (41, 42). In the free enzyme and in the BH_4-bound complex, the ligands to the ferrous iron are two histidine residues, one monodentate glutamate residue, and three waters (41). The pterin forms hydrogen bonds to backbone atoms and water-mediated hydrogen bonds to Glu286. In the ternary complex with BH_4 and an amino acid substrate, the glutamate is bidenate and the iron has lost two water molecules (42, 43), leaving a site for the binding of oxygen. The pterin has moved 2.6 Å from its position in the binary complex, closer to the iron and forming direct hydrogen bonds with Glu286. There is also a change in the position of a surface loop consisting of residues 131–150. In the binary structure, the loop is in an open position, with the side chain of Tyr138 over 20 Å from the iron. In the ternary complex, this loop has closed over the active site opening so that Tyr138 is buried in the active site with its phenolic oxygen within 5 Å of the iron. The homologous loop in rat TyrH (residues 178–193) undergoes a similar rearrangement upon substrate binding (44).

The present data indicate that there are two E-BH_4 complexes, only one of which is productive. The different interactions of BH_4 in the structures of binary and ternary complexes of the ferrous enzyme provide a possible structural basis for this. In going from the binary to the ternary complex, the water molecules that bridge the pterin and Glu286 are lost. If loss of these waters requires dissociation of the pterin, the structure of the enzyme with BH_4 alone would represent the dead-end complex that is detected in our kinetic analysis.[3] It is also possible that the Tyr138 loop is more dynamic in the isolated catalytic domain than indicated by the crystal structures, with the conformation of the loop directly coupled to the binding orientation of BH_4. Productive binding (E'-BH_4) would occur in the open conformation, permitting the binding of phenylalanine to form the ternary complex. The closed conformation would then reflect the inhibitory binding of BH_4 (E"-BH_4), with the concomitant loop closure preventing the addition of phenylalanine to the active site. For productive binding, the loop must reopen, releasing the pterin and restoring the free enzyme.

There is precedent for an unproductive mode for the binding of BH_4 to intact PheH. In studies of the allosteric properties of PheH, Shiman (9) proposed an inhibitory E-BH_4 complex distinct from that involved in catalysis; in this model the inhibited enzyme could not be activated by phenylalanine until the pterin dissociated. A structural explanation for the inhibition has been proposed in which Ser23 of the regulatory domain forms a hydrogen bond with the dihydroxypropyl side chain of BH_4 when it is bound in the mode seen in structures of the E-BH_4 complex, thereby stabilizing the inactive form of the enzyme (45). This interaction is not possible with the E-BH_4-phenylalanine complex due to the altered position of BH_4.

The binding of phenylalanine to the free enzyme produces a dead-end E-Phe complex, with a K_d value (1300 μM) ten-fold that for phenylalanine binding productively to E'-BH_4. Substrate inhibition by phenylalanine has not been reported for intact eukaryotic PheH (6, 46); however, substrate inhibition by the amino acid substrate has been seen in TyrH (47–49), the catalytic domain of TrpH (21), and bacterial PheH (50). A straightforward explanation for the dead-end complex of PheH with phenylalanine is that the formation of

[3]Variations on the kinetic mechanisms in Schemes 4 and 5 were considered in which the different E-BH_4 complexes were reversibly connected without the need for dissociation of the BH_4. In fitting these mechanisms to the data, they invariably collapsed to the simpler schemes lacking a reversible connection.

the E-Phe complex results in closure of the Tyr138 loop, preventing the binding of BH_4 to generate a productive ternary complex. It is also possible that at high concentrations, phenylalanine can occupy an alternative location such as the pterin binding site, which would directly inhibit pterin binding.

The results presented here support the binding of pterin before the amino acid substrate in the overall kinetic mechanism. The steady-state kinetic mechanism has not been determined for a eukaryotic PheH. Previous studies of the kinetic mechanism for bacterial PheH have given contradictory results for the order of binding. Pember et al. (51) concluded that oxygen binds first followed by a random addition of pterin or phenylalanine. In contrast, Volner et al. (50), concluded that pterin binds first followed by phenylalanine, with oxygen binding last. The latter agrees with the present results. TyrH also shows a binding order with the pterin binding first (52), indicating this may be a common feature for this family of enzymes.

The hydroxylation reaction is initiated by the rapid, reversible addition of oxygen to the ternary complex. Previous rapid-reaction studies with TyrH (53) and TrpH (54) also found evidence for reversible O_2 binding to these enzymes. The reaction of the PheHΔ117 ternary complex with O_2 to form the initial O_2-bound intermediate occurs in the dead-time of the stopped-flow instrument so that it is not seen directly, but it is apparent as a shift in the initial absorbance with increasing concentrations of O_2. After oxygen binds, the next step in the reaction with BH_4 as the pterin substrate is marked by an absorbance increase at 248 nm. This could suggest the formation of 4a-HO-BH_3 and the Fe(IV)O; however, a large decrease in absorbance at 340 nm is also observed in this step. In the reaction with $6MPH_4$ as the pterin substrate, the step immediately following binding of O_2 to the ternary complex is similarly associated with a decrease in the absorbance at 340 nm, but little change at the other wavelengths. As changes at 340 nm reflect the formation of the various pterin binding complexes and are not associated with formation of the 4a-hydroxypterin intermediate, it is more likely that this step indicates the formation of a discrete complex such as the proposed Fe(II)-peroxypterin intermediate (20) in reactions with either pterin. An intermediate prior to formation of Fe(IV)O has also been seen in stopped-flow experiments in TrpH (54). In the reaction with $6MPH_4$, the absorbance increase at 248 nm and the decrease at 318 nm associated with 4a-hydroxypterin formation are only observed in the second step following O_2 binding, indicating that formation of the 4a-hydroxypterin and the Fe(IV)O intermediate occurs in this step. In the reaction with BH_4, the absorbance at 248 nm also increases in this step, such that the total magnitude of the increase in absorbance at this wavelength is identical to that seen in the reaction with $6MPH_4$. This strongly suggests that formation of the 4a-hydroxypterin and Fe(IV)O also occurs in the second step following O_2 binding in the reaction with BH_4. PheHΔ117 shows a preference for the physiological pterin with a value for the rate constant for this step three-fold that for $6MPH_4$. As structural differences between the two pterins are restricted to the side-chain at the 6-position, substituent effects would be expected to show little discrimination, so that it is likely the differences in the rates arise from differences in the orientations of the pterins.

With both BH_4 and $6MPH_4$, the value for the rate constant for the second step after O_2 binding (k_7) shows reasonable agreement with the rate constant for the burst of tyrosine formation in the chemical-quench experiments, so that this step can be assigned as hydroxylation of the amino acid by the Fe(IV)O intermediate. As this step was also assigned to the formation of the Fe(IV)O intermediate, amino acid hydroxylation must be faster than the formation of Fe(IV)O. In the case of TyrH, rapid-quench Mössbauer spectroscopy has established directly that the Fe(IV)O reacts more rapidly than it forms (31).

The similarity in the values for the rate constant for the final step and the k_{cat} values from the chemical-quench data support this step as being product release, so that k_{cat} for PheHΔ117 is principally determined by the rate of product release. Rate-determining product release is also seen with both TyrH (55) and TrpH (54), arguing for this as a common feature for this family of enzymes.

This study presents a complete kinetic mechanism for PheHΔ117. Substrate binding is ordered with pterin binding first followed by phenylalanine. Both substrates can bind the free enzyme to produce dead-end complexes that must dissociate to allow productive assembly of the ternary complex. The dead-end enzyme-BH_4 complex is a significant binding mode for BH_4 with on and off rate constants similar to those for the productive binding mode. This complex is proposed to represent the inhibitory orientation of BH_4 in the intact enzyme. Phenylalanine binds much more weakly to the free enzyme, and the resulting complex is not expected to be relevant under physiological conditions. Molecular oxygen binds to the ternary complex in a rapid equilibrium prior to the formation of an unidentified intermediate detectable as a loss of absorbance at 340 nm. Slow decay of this intermediate yields the reactive Fe(IV)O species that rapidly hydroxylates the amino acid. Product release is the slowest step in the reaction and the rate-determining step for enzyme turnover.

Supplementary Material

Refer to Web version on PubMed Central for supplementary material.

Acknowledgments

We thank Dr. Ken Johnson of the University of Texas for many helpful discussions in the use of KinTek Explorer and FitSpace Explorer.

ABBREVIATIONS

PheH	phenylalanine hydroxylase
BH_4	tetrahydrobiopterin
LB-amp	Luria-Bertani broth containing 100 μg/ml ampicillin
PMSF	phenylmethylsulfonyl fluoride
IPTG	isopropyl-β-D-thiogalactopyranoside
6MPH_4	6-methyltetrahydropterin

REFERENCES

1. Fitzpatrick PF. The tetrahydropterin-dependent amino acid hydroxylases. Ann. Rev. Biochem. 1999; 68:355–381. [PubMed: 10872454]
2. Bailey SW, Rebrin I, Boerth SR, Ayling JE. Synthesis of 4a-hydroxytetrahydropterins and the mechanism of their nonenzymatic dehydration to quinoid dihydropterins. J. Am. Chem. Soc. 1995; 117:10203–10211.
3. Williams RA, Mamotte CDS, Burnett JR. Phenylketonuria: An Inborn Error of Phenylalanine Metabolism. Clin. Biochem. Rev. 2008; 29:31–41. [PubMed: 18566668]
4. Fitzpatrick PF. Allosteric regulation of phenylalanine hydroxylase. Arch. Biochem. Biophys. 2012; 519:194–201. [PubMed: 22005392]
5. Nielsen KH. Rat Liver Phenylalanine Hydroxylase. Eur. J. Biochem. 1969; 7:360–369. [PubMed: 5791581]

6. Shiman R, Gray DW. Substrate activation of phenylalanine hydroxylase. A kinetic characterizaion. J. Biol. Chem. 1980; 255:4793–4800. [PubMed: 7372612]
7. Li J, Ilangovan U, Daubner SC, Hinck AP, Fitzpatrick PF. Direct Evidence for a Phenylalanine Site in the Regulatory Domain of Phenylalanine Hydroxylase. Arch. Biochem. Biophys. 2011; 505:250–255. [PubMed: 20951114]
8. Kobe B, Jennings IG, House CM, Michell BJ, Goodwill KE, Santarsiero BD, Stevens RC, Cotton RGH, Kemp BE. Structural basis of autoregulation of phenylalanine hydroxylase. Nat. Struct. Biol. 1999; 6:442–448. [PubMed: 10331871]
9. Xia T, Gray DW, Shiman R. Regulation of rat liver phenylalanine hydroxylase. III. Control of catalysis by (6R)-tetrahydrobiopterin and phenylalanine. J. Biol. Chem. 1994; 269:24657–24665. [PubMed: 7929137]
10. Daubner SC, Hillas PJ, Fitzpatrick PF. Expression and characterization of the catalytic domain of human phenylalanine hydroxylase. Arch. Biochem. Biophys. 1997; 348:295–302. [PubMed: 9434741]
11. Daubner SC, Hillas PJ, Fitzpatrick PF. Characterization of chimeric pterin-dependent hydroxylases: Contributions of the regulatory domains of tyrosine and phenylalanine hydroxylase to substrate specificity. Biochemistry. 1997; 36:11574–11582. [PubMed: 9305947]
12. Ledley FD, DiLella AG, Kwok SLM, Woo SLC. Homology between phenylalanine and tyrosine hydroxylases reveals common structural and functional domains. Biochemistry. 1985; 24:3389–3394. [PubMed: 2412578]
13. Knappskog PM, Flatmark T, Aarden JM, Haavik J, Martinez A. Structure/function relationships in human phenylalanine hydroxylase. Effect of terminal deletions on the oligomerization, activation and cooperativity of substrate binding to the enzyme. Eur. J. Biochem. 1996; 242:813–821. [PubMed: 9022714]
14. Zhao G, Xia T, Song J, Jensen RA. Pseudomonas aeruginosa possesses homologues of mammalian phenylalanine hydroxylase and 4a-carbinolamine dehydratase/DCoH as part of a three-component gene cluster. Proc. Natl. Acad. Sci. U.S.A. 1994; 91:1366–1370. [PubMed: 8108417]
15. Chen D, Frey P. Phenylalanine hydroxylase from *Chromobacterium violaceum*. Uncoupled oxidation of tetrahydropterin and the role of iron in hydroxylation. J. Biol. Chem. 1998; 273:25594–25601. [PubMed: 9748224]
16. Goodwill KE, Sabatier C, Marks C, Raag R, Fitzpatrick PF, Stevens RC. Crystal structure of tyrosine hydroxylase at 2.3 Å and its implications for inherited neurodegenerative diseases. Nat. Struct. Biol. 1997; 4:578–585. [PubMed: 9228951]
17. Erlandsen H, Fusetti F, Martinez A, Hough E, Flatmark T, Stevens RC. Crystal structure of the catalytic domain of human phenylalanine hydroxylase reveals the structural basis for phenylketonuria. Nat. Struct. Biol. 1997; 4:995–1000. [PubMed: 9406548]
18. Wang L, Erlandsen H, Haavik J, Knappskog PM, Stevens RC. Three-dimensional structure of human tryptophan hydroxylase and its implications for the biosynthesis of the neurotransmitters serotonin and melatonin. Biochemistry. 2002; 41:12569–12574. [PubMed: 12379098]
19. Hegg EL, Que L. The 2-His-1-carboxylate facial triad - An emerging structural motif in mononuclear non-heme iron (II) enxymes. Eur. J. Biochem. 1997; 250:625–629. [PubMed: 9461283]
20. Fitzpatrick PF. Mechanism of aromatic amino acid hydroxylation. Biochemistry. 2003; 42:14083–14091. [PubMed: 14640675]
21. Moran GR, Daubner SC, Fitzpatrick PF. Expression and characterization of the catalytic core of tryptophan hydroxylase. J. Biol. Chem. 1998; 273:12259–12266. [PubMed: 9575176]
22. Daubner SC, Melendez J, Fitzpatrick PF. Reversing the substrate specificities of phenylalanine and tyrosine hydroxylase: Aspartate 425 of tyrosine hydroxylase is essential for L-DOPA formation. Biochemistry. 2000; 39:9652–9661. [PubMed: 10933781]
23. McKinney J, Teigen K, Frøystein NA, Salaün C, Knappskog PM, Haavik J, Martínez A. Conformation of the substrate and pterin cofactor bound to human tryptophan hydroxylase. Important role of Phe313 in substrate specificity. Biochemistry. 2001; 40:15591–15601. [PubMed: 11747434]

24. Daubner SC, Moran GR, Fitzpatrick PF. Role of tryptophan hydroxylase Phe313 in determining substrate specificity. Biochem. Biophys. Res. Commun. 2002; 292:639–641. [PubMed: 11922614]
25. Hillas PJ, Fitzpatrick PF. A mechanism for hydroxylation by tyrosine hydroxylase based on partitioning of substituted phenylalanines. Biochemistry. 1996; 35:6969–6975. [PubMed: 8679520]
26. Daubner SC, Fitzpatrick PF. Site-directed mutants of charged residues in the active site of tyrosine hydroxylase. Biochemistry. 1999; 38:4448–4454. [PubMed: 10194366]
27. Ellis HR, Daubner SC, McCulloch RI, Fitzpatrick PF. Phenylalanine residues in the active site of tyrosine hydroxylase: Mutagenesis of Phe300 and Phe309 to alanine and metal ion-catalyzed hydroxylation of Phe300. Biochemistry. 1999; 38:10909–10914. [PubMed: 10460145]
28. Ellis HR, Fitzpatrick PF. Identification of a serine residue involved in stabilization of the iron ligand histidine 331 in tyrosine hydroxylase. J. Inorg. Biochem. 1999; 74:123–123.
29. Fitzpatrick PF, Ralph EC, Ellis HR, Willmon OJ, Daubner SC. Characterization of metal ligand mutants of tyrosine hydroxylase: insights into the plasticity of a 2-histidine-1-carboxylate triad. Biochemistry. 2003; 42:2081–2088. [PubMed: 12590596]
30. Davis MD, Kaufman S. Products of the tyrosine-dependent oxidation of tetrahydrobiopterin by rat liver phenylalanine hydroxylase. Arch. Biochem. Biophys. 1993; 304:9–16. [PubMed: 8323303]
31. Eser BE, Barr EW, Frantom PA, Saleh L, Bollinger JM Jr, Krebs C, Fitzpatrick PF. Direct spectroscopic evidence for a high-spin Fe(IV) intermediate in tyrosine hydroxylase. J. Am. Chem. Soc. 2007; 129:11334–11335. [PubMed: 17715926]
32. Panay AJ, Lee M, Krebs C, Bollinger JM Jr, Fitzpatrick PF. Evidence for a high spin Fe(IV) species in the catalytic cycle of a bacterial phenylalanine hydroxylase. Biochemistry. 2011; 50:1928–1933. [PubMed: 21261288]
33. Renson JD, Daly J, Weissbach H, Witkop B, Udenfriend S. Enzymatic conversion of 5-tritiotryptophan to 4-tritio-5-hydroxytryptophan. Biochem. Biophys. Res. Commun. 1966; 25:504–513.
34. Guroff G, Levitt M, Daly J, Udenfriend S. The production of meta-tritiotyrosine from p-tritio-phenylalanine by phenylalanine hydroxylase. Biochem. Biophys. Res. Commun. 1966; 25:253–259. [PubMed: 5971770]
35. Moran GR, Derecskei-Kovacs A, Hillas PJ, Fitzpatrick PF. On the catalytic mechanism of tryptophan hydroxylase. J. Am. Chem. Soc. 2000; 122:4535–4541.
36. Frantom PA, Fitzpatrick PF. Uncoupled forms of tyrosine hydroxylase unmask kinetic isotope effects on chemical steps. J. Am. Chem. Soc. 2003; 125:16190–16191. [PubMed: 14692751]
37. Pavon JA, Fitzpatrick PF. Insights into the catalytic mechanisms of phenylalanine and tryptophan hydroxylase from kinetic isotope effects on aromatic hydroxylation. Biochemistry. 2006; 45:11030–11037. [PubMed: 16953590]
38. Gottschall DW, Dietrich RF, Benkovic SJ. Phenylalanine hydroxylase. Correlation of the iron content with activity and the preparation and reconstitution of the apoenzyme. J. Biol. Chem. 1982; 257:845–849. [PubMed: 7054185]
39. Johnson KA, Simpson ZB, Blom T. Global Kinetic Explorer: A new computer program for dynamic simulation and fitting of kinetic data. Anal. Biochem. 2009; 387:20–29. [PubMed: 19154726]
40. Johnson KA, Simpson ZB, Blom T. FitSpace Explorer: An algorithm to evaluate multidimensional parameter space in fitting kinetic data. Anal. Biochem. 2009; 387:30–41. [PubMed: 19168024]
41. Andersen OA, Flatmark T, Hough E. High resolution crystal structures of the catalytic domain of human phenylalanine hydroxylase in its catalytically active Fe(II) form and binary complex with tetrahydrobiopterin. J. Mol. Biol. 2001; 314:279–291. [PubMed: 11718561]
42. Andersen OA, Stokka AJ, Flatmark T, Hough E. 2.0 Å Resolution crystal structures of the ternary complexes of human phenylalanine hydroxylase catalytic domain with tetrahydrobiopterin and 3-(2-thienyl)-L-alanine or L-norleucine: substrate specificity and molecular motions related to substrate binding. J. Mol. Biol. 2003; 333:747–757. [PubMed: 14568534]
43. Wasinger EC, Mitić N, Hedman B, Caradonna J, Solomon EI, Hodgson KO. X-Ray absorption spectroscopic investigation of the resting ferrous and cosubstrate-bound active sites of phenylalanine hydroxylase. Biochemistry. 2002; 41:6211–6217. [PubMed: 12009881]

44. Sura GR, Lasagna M, Gawandi V, Reinhart GD, Fitzpatrick PF. Effects of ligands on the mobility of an active-site loop in tyrosine hydroxylase as monitored by fluorescence anisotropy. Biochemistry. 2006; 45:9632–9638. [PubMed: 16878998]
45. Solstad T, Stokka AJ, Andersen OA, Flatmark T. Studies on the regulatory properties of the pterin cofactor and dopamine bound at the active site of human phenylalanine hydroxylase. Eur. J. Biochem. 2003; 270:981–990. [PubMed: 12603331]
46. Martinez A, Knappskog PM, Olafsdottir S, Doskeland AP, Eiken HG, Svebak RM, Bozzini M, Apold J, Flatmark T. Expression of recombinant human phenylalanine hydroxylase as fusion protein in *Escherichia coli* circumvents proteolytic degradation by host cell proteases. Biochem. J. 1995; 306:589–597. [PubMed: 7887915]
47. Shiman R, Akino M, Kaufman S. Solubilization and partial purification of tyrosine hydroxylase from bovine adrenal medulla. J. Biol. Chem. 1971; 246:1330–1340. [PubMed: 5545077]
48. Katz IR, Lloyd T, Kaufman S. Studies on phenylalanine and tyrosine hydroxylation by rat brain tyrosine hydroxylase. Biochim. Biophys. Acta. 1976; 445:567–578. [PubMed: 9989]
49. Fitzpatrick PF, Chlumsky LJ, Daubner SC, O'Malley KL. Expression of rat tyrosine hydroxylase in insect tissue culture cells and purification and characterization of the cloned enzyme. J. Biol. Chem. 1990; 265:2042–2047. [PubMed: 1967606]
50. Volner A, Zoidakis J, Abu-Omar MM. Order of substrate binding in bacterial phenylalanine hydroxylase and its mechanistic implication for pterin-dependent oxygenases. J. Biol. Inorg. Chem. 2003; 8:121–128. [PubMed: 12459906]
51. Pember SO, Johnson KA, Villafranca JJ, Benkovic SJ. Mechanistic studies on phenylalanine hydroxylase from *Chromobacterium violaceum* Evidence for the formation of an enzyme-oxygen complex. Biochemistry. 1989; 28:2124–2130. [PubMed: 2719947]
52. Fitzpatrick PF. The steady state kinetic mechanism of rat tyrosine hydroxylase. Biochemistry. 1991; 30:3658–3662. [PubMed: 1673058]
53. Chow MS, Eser BE, Wilson SA, Hodgson KO, Hedman B, Fitzpatrick PF, Solomon EI. Spectroscopy and kinetics of wild-type and mutant tyrosine hydroxylase: Mechanistic insight into O_2 activation. J. Am. Chem. Soc. 2009; 131:7685–7698. [PubMed: 19489646]
54. Pavon JA, Eser BE, Huynh MT, Fitzpatrick PF. Single turnover kinetics of tryptophan hydroxylase: Evidence for a new intermediate in the reaction of the aromatic amino acid hydroxylases. Biochemistry. 2010; 49:7563–7571. [PubMed: 20687613]
55. Eser BE, Fitzpatrick PF. Measurement of Intrinsic Rate Constants in the Tyrosine Hydroxylase Reaction. Biochemistry. 2010; 49:645–652. [PubMed: 20025246]

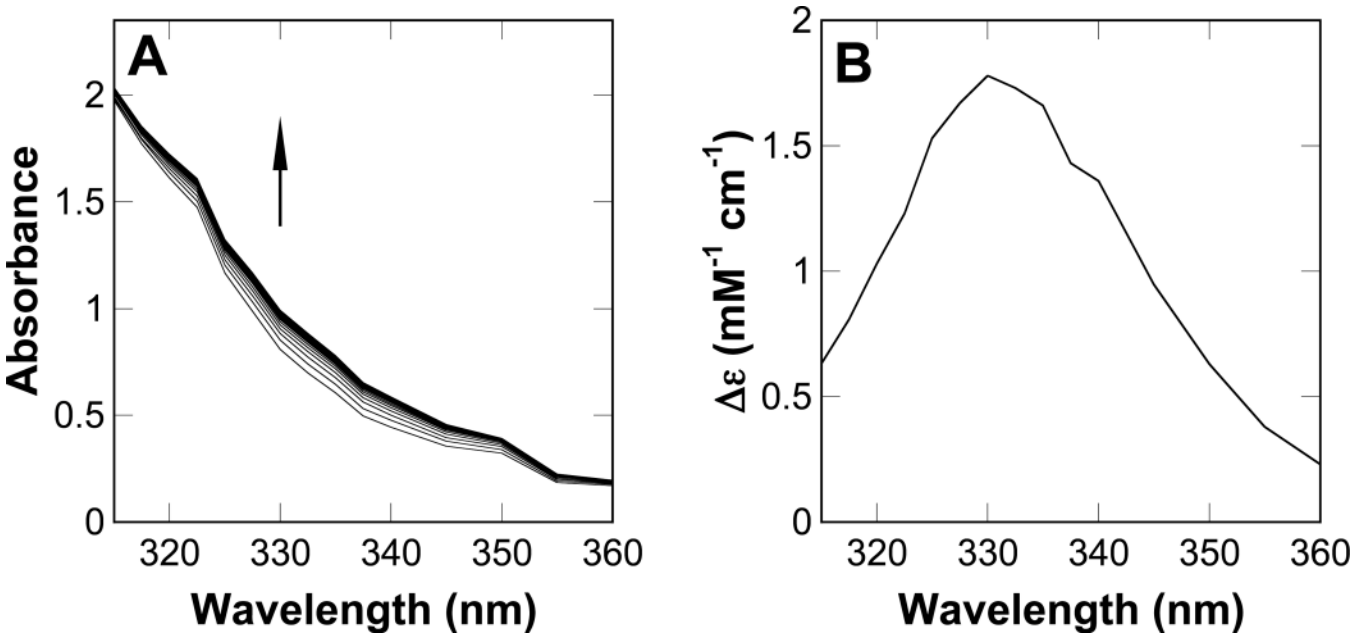

Figure 1.

Absorbance changes upon formation of the PheHΔ117-BH_4-phenylalanine ternary complex. (A) Spectra at 5 ms intervals during the first 100 ms of the anaerobic reaction of 150 μM PheHΔ117 plus 300 μM BH_4 with 3.0 mM phenylalanine at 5 °C. All concentrations are after mixing. (B) The difference spectrum at 1 s.

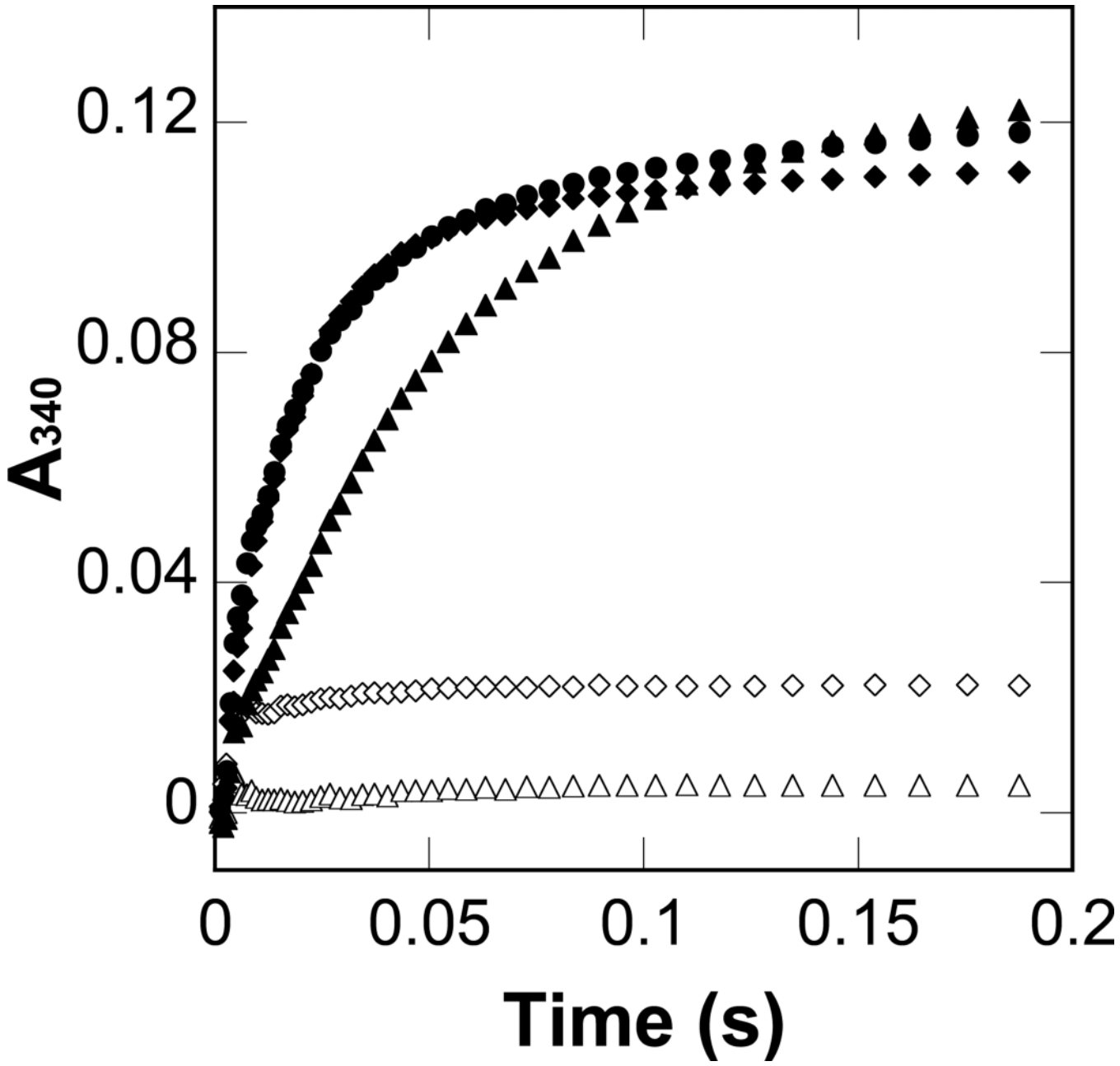

Figure 2.

Absorbance changes during the anaerobic formation of various PheH-substrate complexes at 5 °C: 150 μM PheHΔ117 vs 3.0 mM phenylalanine (open triangles); 150 μM PheHΔ117 vs 1.2 mM BH_4 (open diamonds); 150 μM PheHΔ117 vs 1.2 mM BH_4 plus 3.0 mM phenylalanine (closed circles); 150 μM PheHΔ117 plus 1.2 mM BH_4 vs 3.0 mM phenylalanine (closed diamonds); 150 μM PheHΔ117 plus 3.0 mM phenylalanine vs 1.2 mM BH_4 (closed triangles). (All concentrations are after mixing.) Every fifth point is shown for clarity.

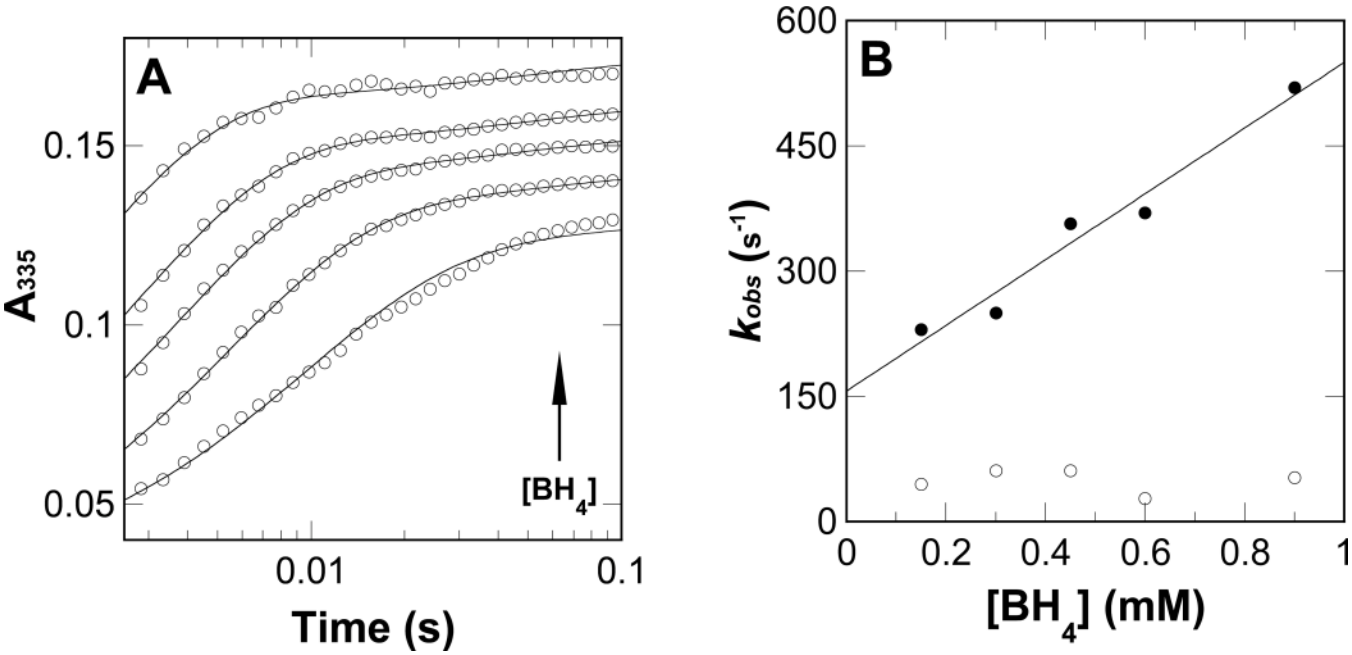

Figure 3.

Kinetics of binding of BH_4 to PheHΔ117. (A) Absorbance changes at 335 nm upon formation of the PheHΔ117-BH_4 binary complex. PheHΔ117 (75 μM) was reacted with 0.15, 0.3, 0.45, 0.6 or 0.9 mM BH_4 at 5 °C. (All concentrations are after mixing.) The individual curves are offset with every second point shown for clarity. The lines are from the kinetic mechanism in Scheme 5C with the rate constants in Table 3. (B) Effect of the concentration of BH_4 on the values of k_{1obs} closed circles) and k_{2obs} open circles). The line indicates the fit with eq 2. The rate constants were determined from two-phase fits (eq 1) to the data in A.

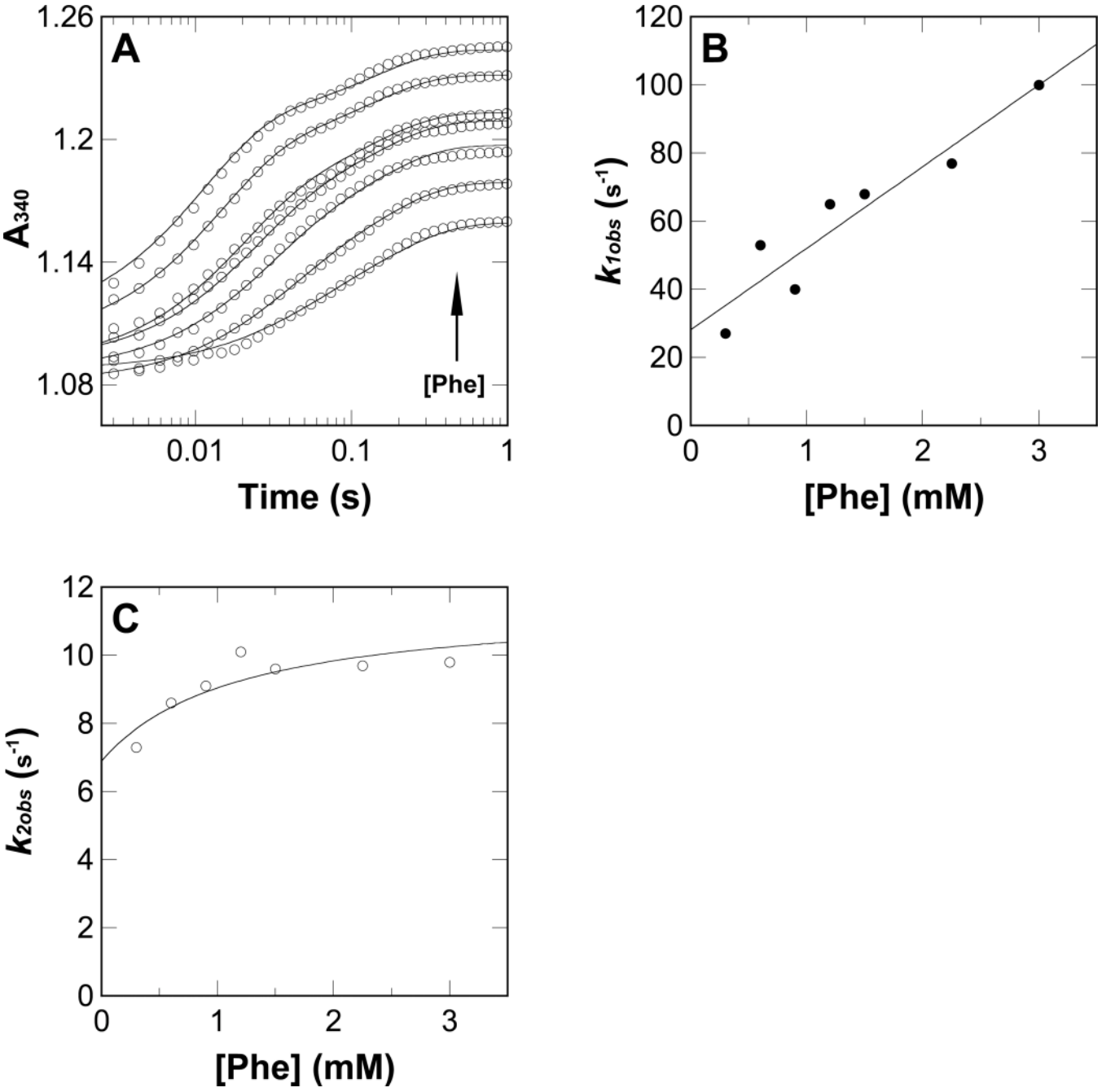

Figure 4.

Kinetics of binding of phenylalanine to PheHΔ117 plus BH_4. (A) Stopped-flow traces showing the formation of the E-BH_4-Phe complex from a preequilibrated mixture of PheHΔ117 and BH_4. A solution of 75 μM PheHΔ117 plus 1.0 mM BH_4 was reacted with 0.3, 0.6, 0.9, 1.2, 1.5, 2.25 or 3.0 mM phenylalanine at 5 °C. (All concentrations are after mixing.) Every third point is shown for clarity. The lines are from the kinetic mechanism in Scheme 5C with the rate constants in Table 3. (B) Effect of the concentration of phenylalanine on the value of k_{1obs}. The line indicates the fit with eq 2. (C) Effect of the concentration of phenylalanine on the value of k_{2obs}. The line indicates the fit with eq 3. The rate constants for B and C were determined from two-phase fits (eq 1) to the data in A.

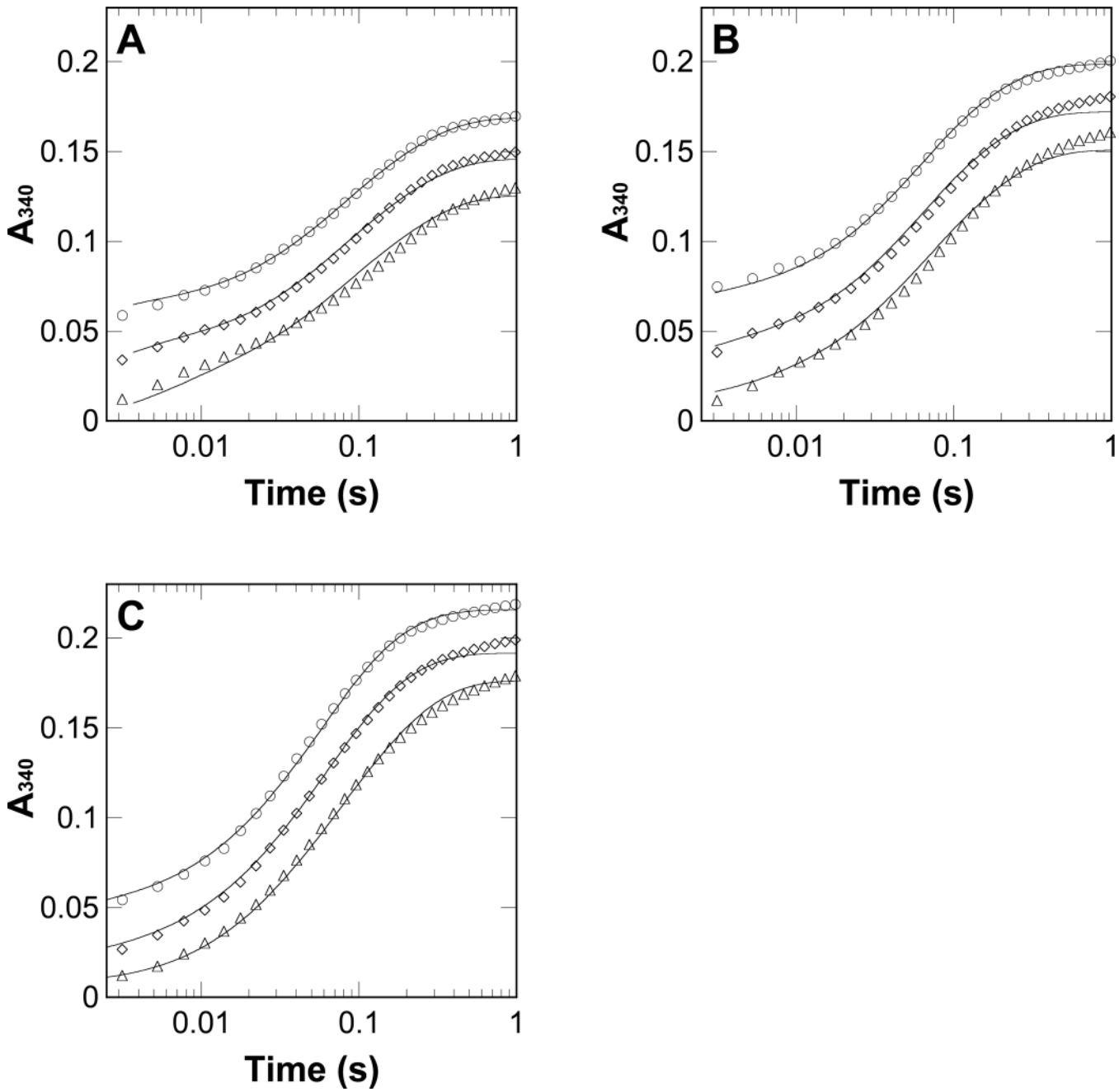

Figure 5.

Stopped-flow traces showing the formation of the PheHΔ117-BH_4-phenylalanine ternary complex from an enzyme-phenylalanine complex. PheHΔ117 (75 μM) plus 0.3 (triangles), 0.9 (diamonds) or 3.0 mM phenylalanine (circles) was reacted with 0.3 (A), 0.9 (B) or 1.5 mM (C) BH_4 at 5 °C. (All concentrations are after mixing.) The individual curves are offset with every third point shown for clarity. The lines are from the kinetic mechanism in Scheme 5C with the rate constants in Table 3.

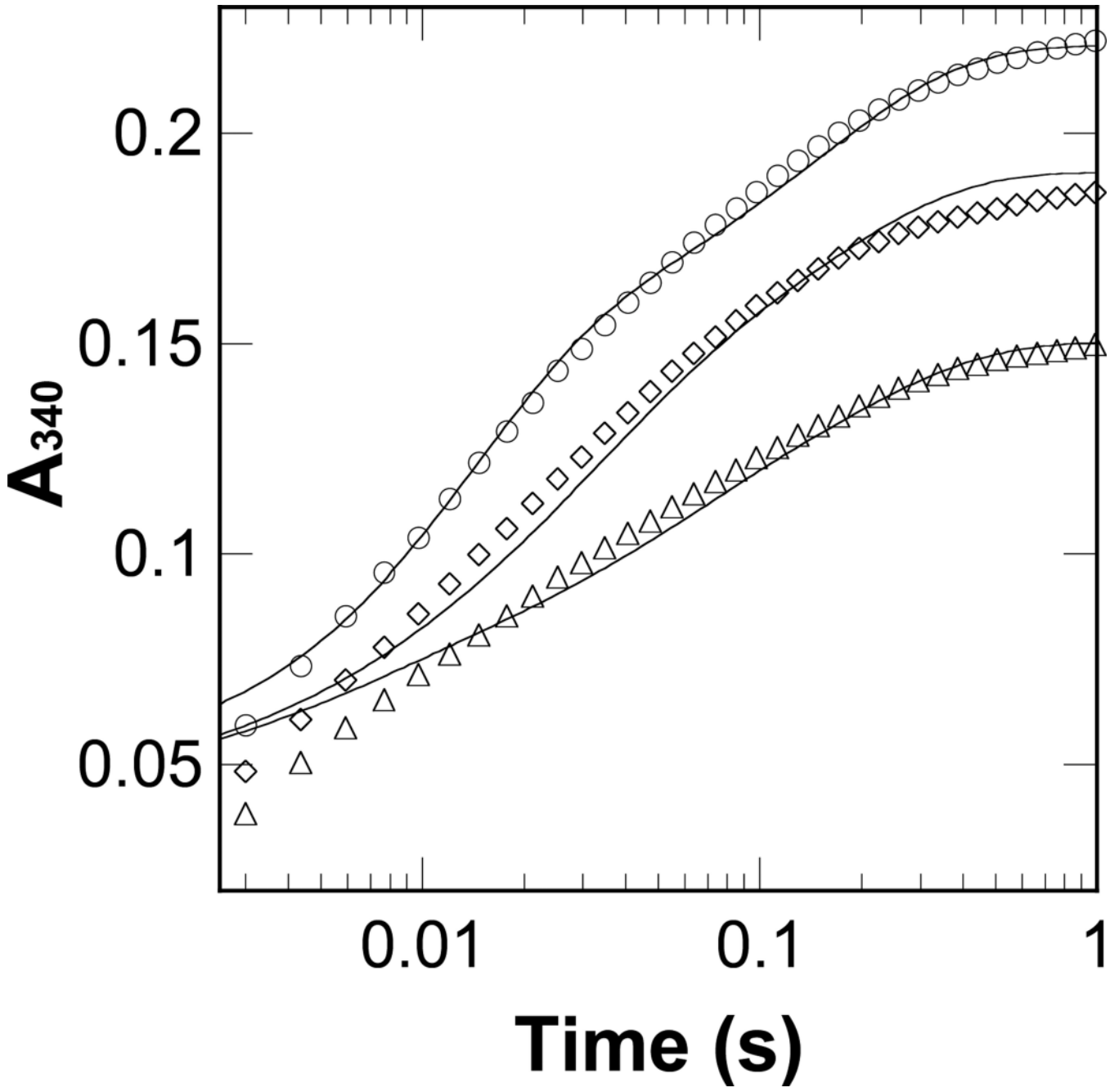

Figure 6.

Stopped-flow traces showing the formation of the PheHΔ117-BH_4-phenylalanine ternary complex by addition of BH_4 and phenylalanine to free enzyme. A solution containing 0.3 mM BH_4 plus 0.3 (triangles), 0.9 (diamonds) or 3.0 mM phenylalanine (circles) was reacted anaerobically with 75 μM PheHΔ117 at 5 °C. (All concentrations are after mixing.) The individual curves are offset with every third point shown for clarity. The lines are from the kinetic mechanism in Scheme 5C with the rate constants in Table 3.

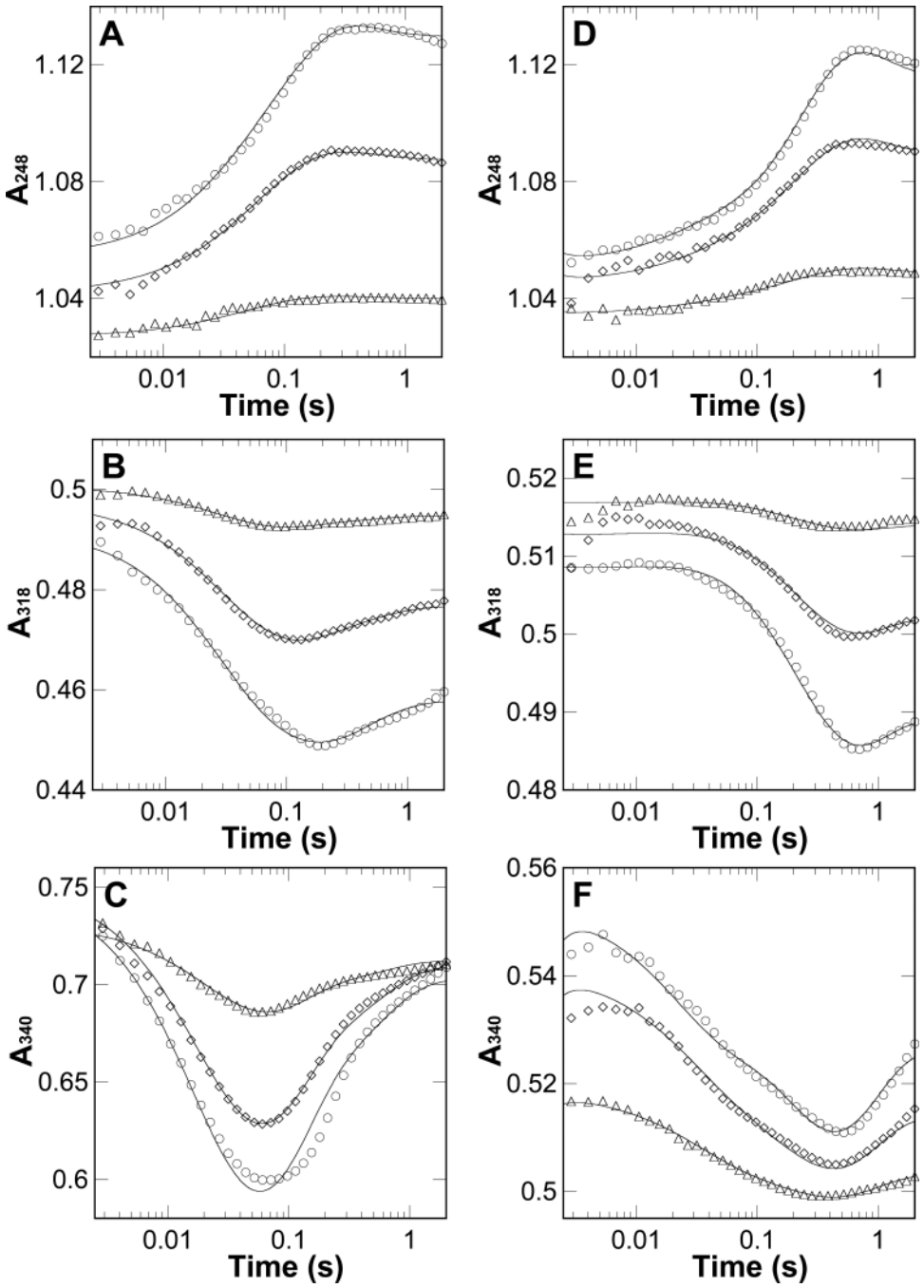

Figure 7.

Stopped-flow traces for the PheHΔ117 hydroxylation reaction. A solution of 75 μM PheHΔ117, 0.3 mM tetrahydropterin and 3.0 mM phenylalanine was mixed with 10 (triangles), 35 (diamonds) or 55 μM O_2 (circles) at 5 °C. (All concentrations are after mixing.) Traces were offset with every third point shown for clarity. (A–C) Traces with BH_4. The lines are from fits with Scheme 6A and the rate constants in Table 4. (D–F) Traces with $6MPH_4$. The lines are from the mechanism in Scheme 6B and the rate constants in Table 4.

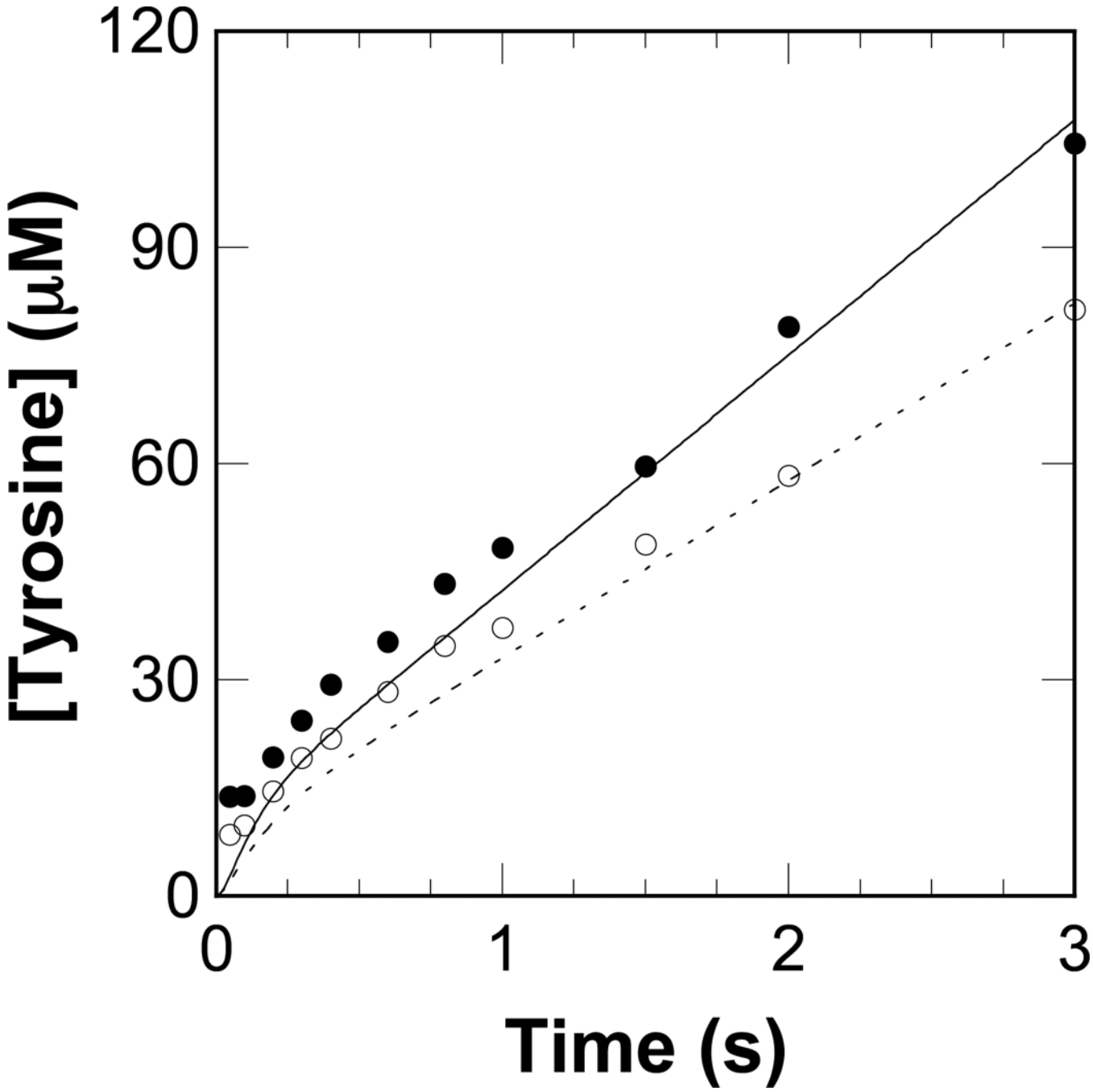

Figure 8.

Tyrosine formation in reactions with BH_4 (closed circles) or $6MPH_4$ (open circles) determined by chemical-quench. A solution of 20 μM PheHΔ117 plus 1.0 mM tetrahydropterin was mixed with a solution of 2.0 mM phenylalanine plus 950 μM O_2 at 5 °C. (All concentrations are after mixing.) The solid line is from the kinetic mechanism in Scheme 6A. The dashed line is from the kinetic mechanism in Scheme 6B. The rate constants used to generate both lines are in Table 4.

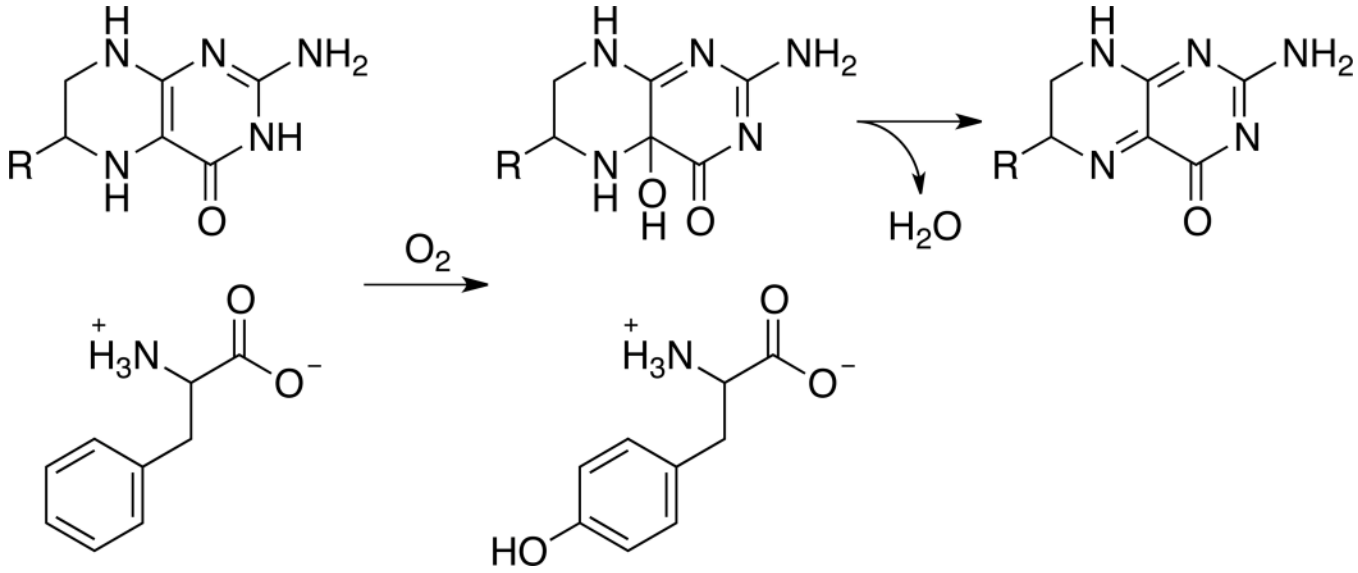

Scheme 1.

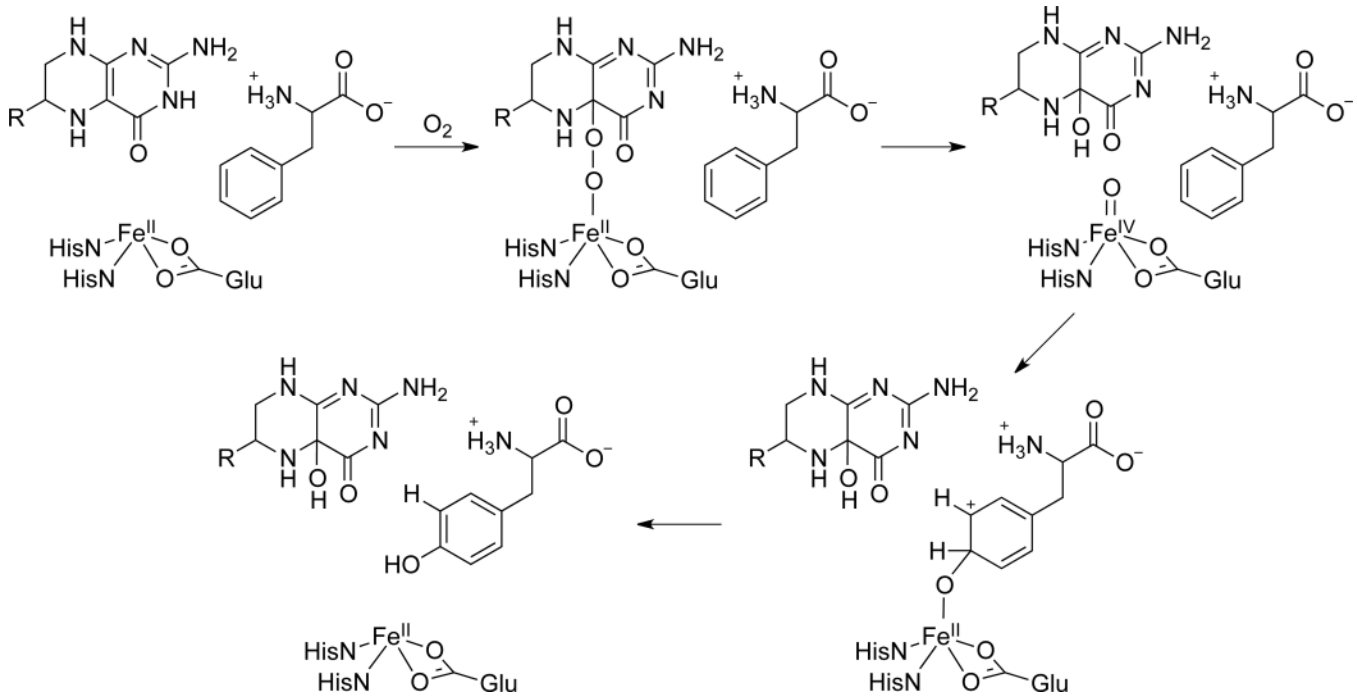

Scheme 2.

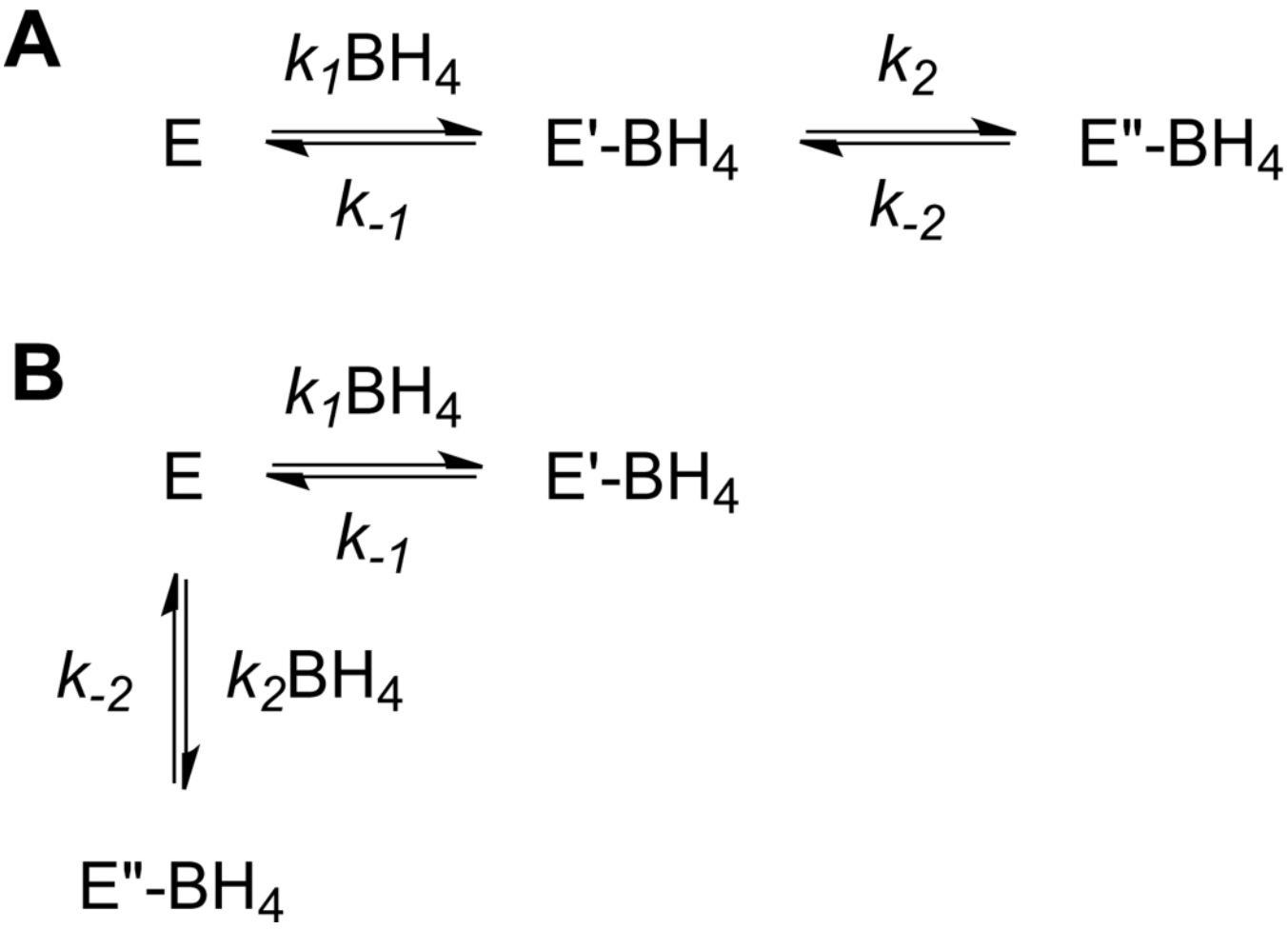

Scheme 3.
Alternative kinetic mechanisms for binding of BH_4 to PheHΔ117: A, sequential mechanism; B, branched mechanism.

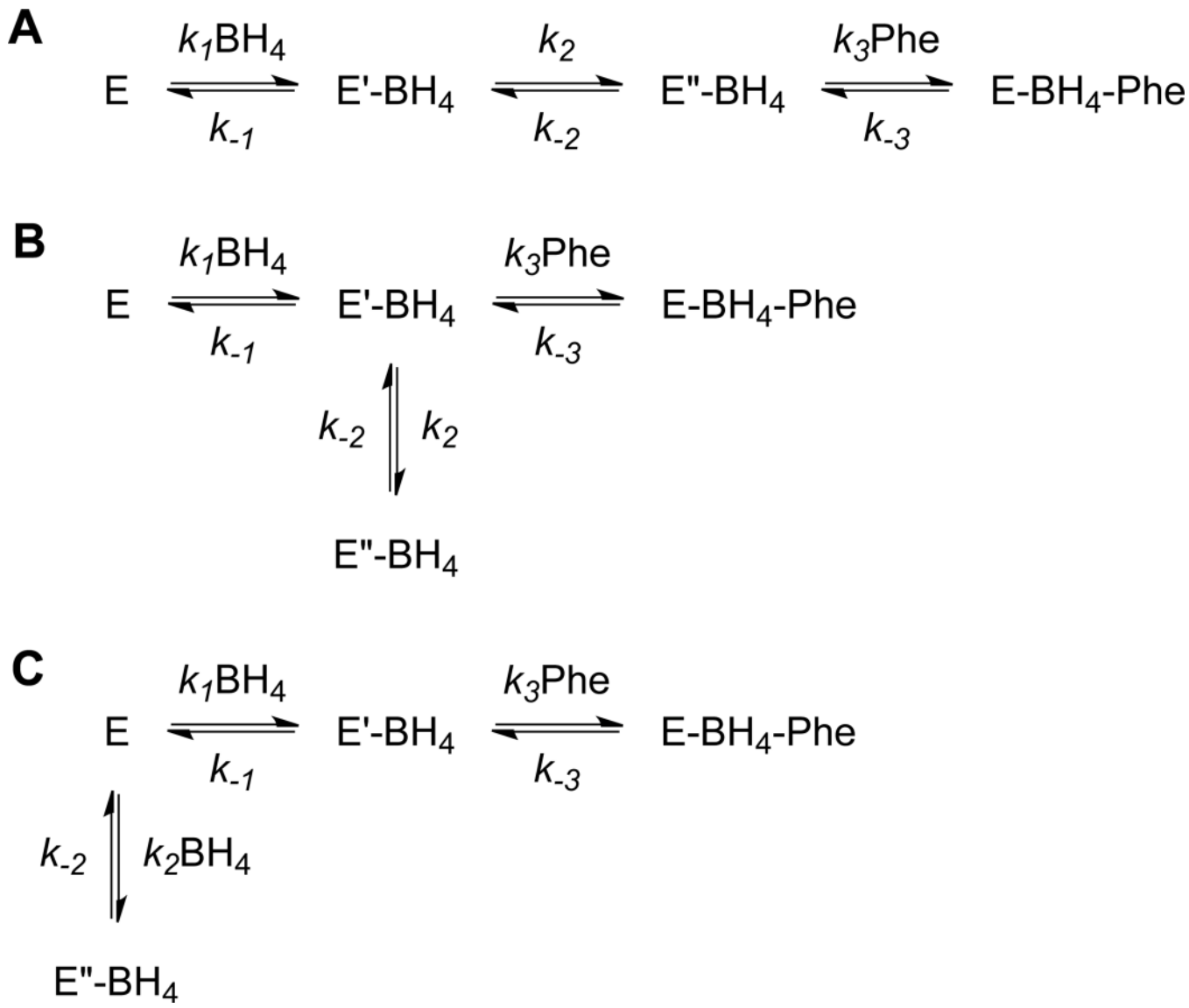

Scheme 4.
Kinetic mechanisms for substrate binding by PheHΔ117.

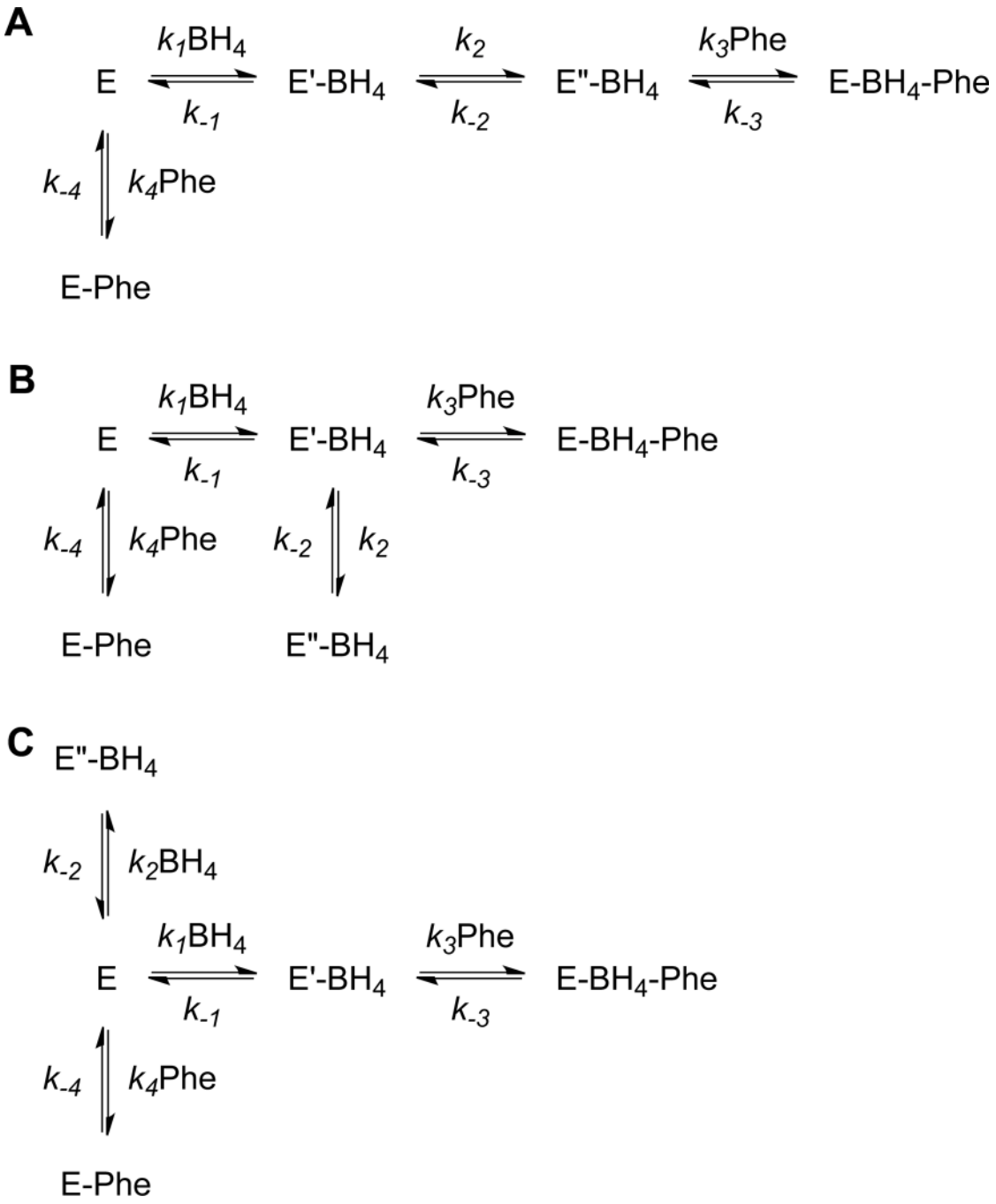

Scheme 5.
Kinetic mechanisms for substrate binding by PheHΔ117 including an enzymephenylalanine complex.

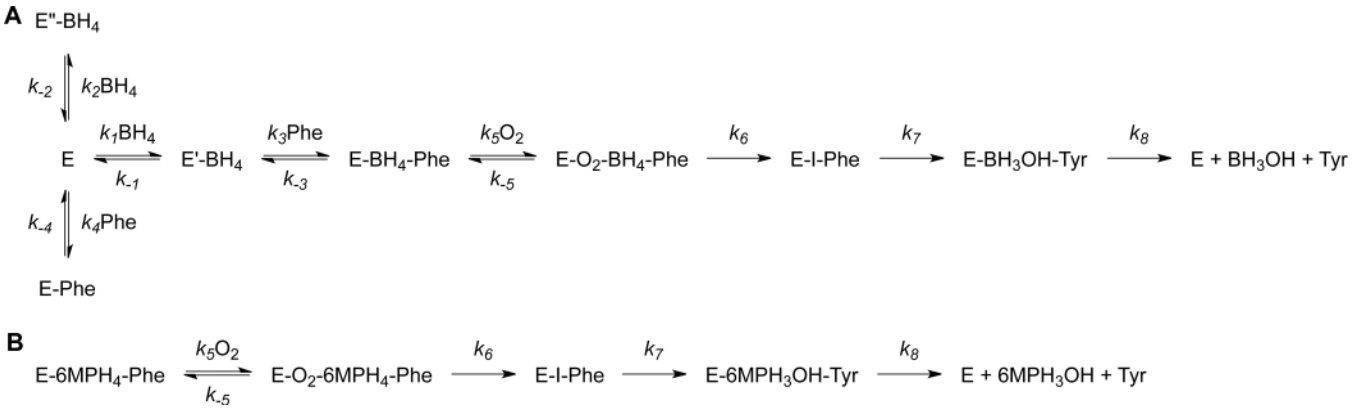

Scheme 6.
Kinetic mechanisms for PheHΔ117.

Table 1

Kinetic parameters for binding of BH_4 to PheHΔ117

kinetic parameter	Scheme 3A	Scheme 3B
k_1	0.59 μM^{-1} s^{-1}	0.33 μM^{-1} s^{-1}
	(0.55 – 0.64)[a]	(0.26 – 0.39)
k_{-1}	46 s^{-1}	12 s^{-1}
	(32 – 66)	(7 – 16)
k_2	32 s^{-1}	0.26 μM^{-1} s^{-1}
	(16 – 52)	(0.20 – 0.31)
k_{-2}	23 s^{-1}	90 s^{-1}
	(13 – 33)	(57 – 140)
X^2	667	667

[a]The values in parentheses are the confidence intervals calculated by FitSpace at a X^2 threshold of 1.15.

Table 2

Kinetic parameters for the kinetic mechanisms in Schemes 4A–C determined globally from the data in Figures 3A and 4A.

kinetic parameter	Scheme 4A	Scheme 4B	Scheme 4C
k_1	0.56 μM^{-1} s^{-1}	0.57 μM^{-1} s^{-1}	0.23 μM^{-1} s^{-1}
	(0.52 – 0.62)[a]	(0.52 – 0.62)	(0.14 – 0.45)
k_{-1}	28 s^{-1}	28 s^{-1}	12 s^{-1}
	(18 – 39)	(18 – 42)	(5 – 33)
k_2	12 s^{-1}	12 s^{-1}	0.34 μM^{-1} s^{-1}
	(9 – 15)	(7 – 19)	(0.14 – 0.44)
k_{-2}	11 s^{-1}	11 s^{-1}	26 s^{-1}
	(6 – 17)	(9 – 14)	(11 – 40)
k_3	0.030 μM^{-1} s^{-1}	0.032 μM^{-1} s^{-1}	0.029 μM^{-1} s^{-1}
	(0.027 – 0.034)	(0.029 – 0.037)	(0.026 – 0.033)
k_{-3}	4.6 s^{-1}	4.5 s^{-1}	4.8 s^{-1}
	(3.9 – 5.5)	(3.8 – 5.3)	(4.0 – 6.2)
X^2	3960	3920	4400

[a]The values in parentheses indicate confidence intervals calculated by FitSpace at a X^2 threshold of 1.07.

Table 3

Kinetic parameters for the kinetic mechanisms in Schemes 5A–C determined globally from the data from Figures 3A, 4A, 5 and 6.

kinetic parameter	Scheme 5A	Scheme 5B	Scheme 5C
k_1	0.69 μM^{-1} s^{-1}	0.56 μM^{-1} s^{-1}	0.31 μM^{-1} s^{-1}
	(0.42 – 1.1)[a]	(0.46 – 0.69)	(0.27 – 0.36)
k_{-1}	120 s^{-1}	32 s^{-1}	20 s^{-1}
	(50 – 730)	(16 – 57)	(14 – 29)
k_2	86 s^{-1}	3.9 s^{-1}	0.27 μM^{-1} s^{-1}
	(30 – 510)	(1.2 – 12)	(0.23 – 0.32)
k_{-2}	52 s^{-1}	12 s^{-1}	19 s^{-1}
	(18 – 200)	(7 – 20)	(14 – 26)
k_3	0.033 μM^{-1} s^{-1}	0.027 μM^{-1} s^{-1}	0.026 μM^{-1} s^{-1}
	(0.022 – 0.054)	(0.022 – 0.034)	(0.022 – 0.030)
k_{-3}	3.6 s^{-1}	4.5 s^{-1}	3.5 s^{-1}
	(2.7 – 4.9)	(3.3 – 6.0)	(3.0 – 4.2)
k_4	0.0030 μM^{-1} s^{-1}	0.015 μM^{-1} s^{-1}	0.016 μM^{-1} s^{-1}
	(0.0004 – 0.015)	(0.009 – 0.026)	(0.010 – 0.024)
k_{-4}	10 s^{-1}	15 s^{-1}	21 s^{-1}
	(4 – 18)	(12 – 19)	(18 – 25)
X^2	38,200	26,000	15,500

[a]The values in parentheses indicate confidence intervals reported by FitSpace at a X^2 threshold of 1.06.

Table 4

Kinetic parameters for the kinetic mechanisms in Schemes 6A and 6B determined globally from the data from Figures 7 and 8.

kinetic parameter	Scheme 6A (BH_4)	Scheme 6B ($6MPH_4$)
k_5[a]	26 μM^{-1} s^{-1}	20 μM^{-1} s^{-1}
k_{-5}[a]	5700 s^{-1}	330 s^{-1}
k_6	140 s^{-1} (67 – 200)[b]	42 s^{-1} (26 – 72)
k_7	13 s^{-1} (8 – 35)	3.9 s^{-1} (2.3 – 5.9)
k_8	2.3 s^{-1} (1.8 – 3.3)	1.9 s^{-1} (1.2 – 3.8)

[a] Values were fixed during the FitSpace calculations.

[b] The values in parentheses indicate confidence intervals reported by FitSpace at a X^2 threshold of 1.1.